Drug Design, Development and Therapy

Dovepress
Taylor & Francis Group

Open Access Full Text Article

ORIGINAL RESEARCH

Mannosamine-Engineered Nanoparticles for Precision Rifapentine Delivery to Macrophages: Advancing Targeted Therapy Against Mycobacterium Tuberculosis

Haopeng Luan*, Cong Peng*, Parhat Yasin, Qisong Shang, Wei Xiang, Xinghua Song

Department of Spine Surgery, the Sixth Affiliated Hospital of Xinjiang Medical University, Urumqi, Xinjiang, 830002, People's Republic of China

*These authors contributed equally to this work

Correspondence: Xinghua Song, Tel +86 13199836661, Email songxinghua19@163.com

Background: Tuberculosis, caused by Mycobacterium tuberculosis (Mtb), remains one of the leading causes of death among infectious diseases. Enhancing the ability of anti-tuberculosis drugs to eradicate Mycobacterium tuberculosis within host cells remains a significant challenge.

Methods: A mannosamine-modified nanoparticle delivery system was developed using poly(lactic-co-glycolic acid) (PLGA) copolymers to enhance the targeted delivery of rifapentine (RPT) to macrophages. D-mannosamine was conjugated to PLGA-polyethylene glycol (PLGA-PEG) copolymers through EDC/NHS coupling chemistry, and the resultant RPT-MAN-PLGA-PEG nanoparticles (NPs) were prepared through a combination of phacoemulsification and solvent evaporation methods. The physicochemical properties, toxicity, in vitro drug release profiles, stability, cellular uptake, and anti-TB efficacy of the NPs were systematically evaluated.

Results: The RPT-MAN-PLGA-PEG NPs had a mean particle size of 108.2 ± 7.2 nm, with encapsulation efficiency and drug loading rates of 81.2 ± 6.3% and 13.7 ± 0.7%, respectively. RPT release from the NPs was sustained for over 60 hours. Notably, the phagocytic uptake of the MAN-PLGA NPs by macrophages was significantly higher compared to PLGA-PEG NPs. Both NPs improved pharmacokinetic parameters without inducing significant organ toxicity. The minimum inhibitory concentration for the NPs was 0.047 μg/mL, compared to 0.2 μg/mL for free RPT.

Conclusion: The engineered RPT-MAN-PLGA-PEG NPs effectively enhanced macrophage uptake in vitro and facilitated the intracellular clearance of Mtb. This nanoparticle-based delivery system offers a promising approach for improving the precision of anti-TB therapy, extending drug release, optimizing pharmacokinetic profiles, augmenting antimicrobial efficacy, and mitigating drug-related toxicities.

Keywords: anti-tubercular, rifapentine, drug delivery system, nanoparticles, macrophages

Introduction

Tuberculosis (TB) continues to be a major global health challenge. In 2023, the estimated number of TB cases worldwide was 10.8 million, similar to the previous year, reflecting a modest increase from 10.1 million cases in 2020. While the global incidence of TB has decreased by 8.3% since 2015, this progress remains well below the World Health Organization's target of a 50% reduction by 2025. In 2023, approximately 1.25 million people died from TB, a slight decrease from the 1.4 million deaths recorded in 2020 and 2021. However, the continued impact of other epidemics during this period has significantly hindered TB control efforts, contributing to nearly 500,000 additional deaths. These trends underscore the urgent need for enhanced prevention and treatment strategies to achieve global TB elimination goals.[1]

Mycobacterium tuberculosis is a facultative intracellular bacterium that primarily parasitizes macrophages. When it invades macrophages, it remains latent in the host through the following mechanisms: 1) inhibition of phagosome fusion

Received: 25 November 2024
Accepted: 6 March 2025
Published: 19 March 2025

Graphical Abstract

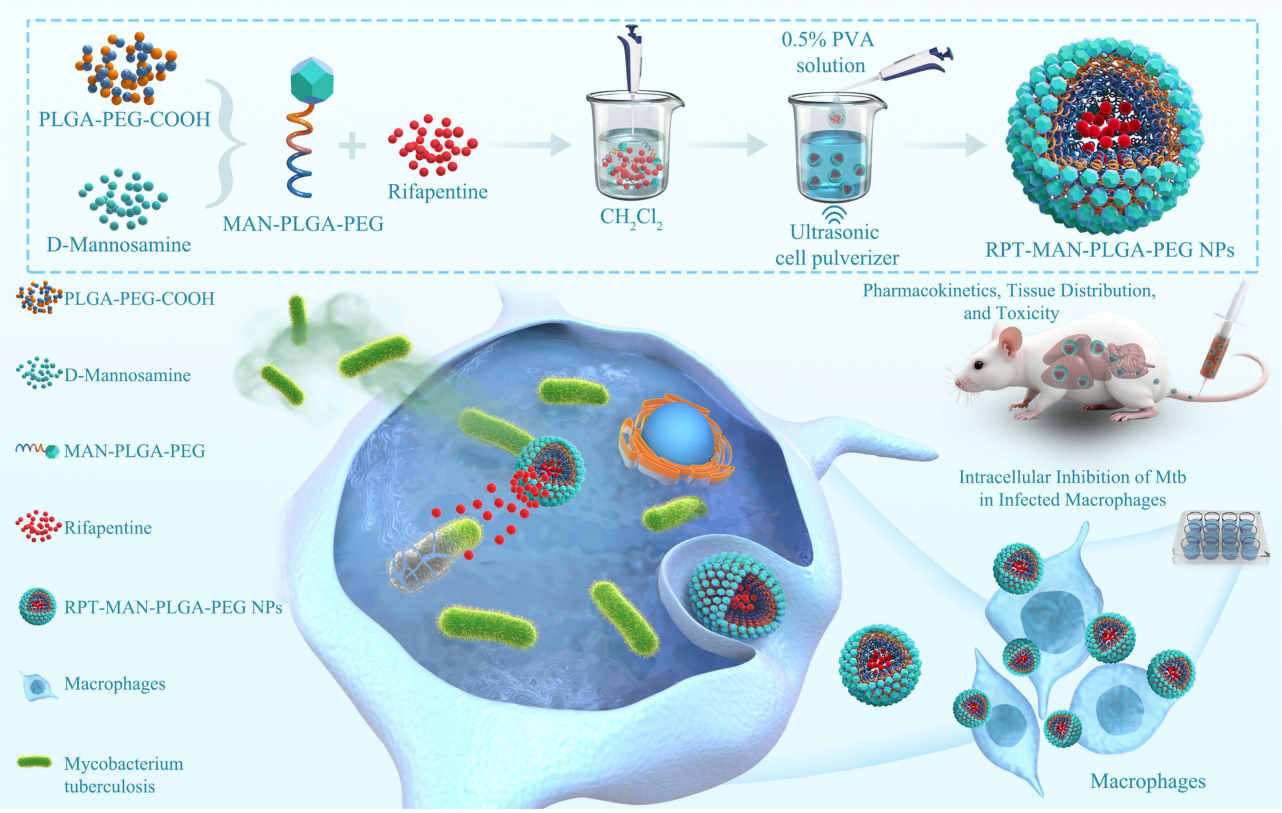

with lysosomes, phagolysosome maturation, and acidification; 2) inhibition of macrophage major histocompatibility complex II (MHC II) gene expression, MHC II molecule maturation, and trafficking; and 3) inhibition of oxidative stress, apoptosis, autophagy, pyroptosis, and metal ion limitation mechanisms.[2] Therefore, eliminating and inhibiting the growth of Mycobacterium tuberculosis within macrophages is crucial for ensuring the successful treatment of tuberculosis.

Currently, first-line anti-tuberculosis drugs are predominantly used in clinical practice. While these drugs effectively kill Mycobacterium tuberculosis, there are still limitations in traditional first-line oral treatments, which include: 1) the requirement for multi-drug combination therapy, prolonged treatment duration, and increased drug resistance; 2) some antibiotics are highly hydrophilic and have poor cell permeability;[3] 3) some antibiotics can easily enter cells, but their intracellular retention time is short; 4) high first-pass metabolism in the liver associated with traditional drug delivery; 5) selective permeability of biological barriers, such as the blood-brain barrier, inhibits the effective delivery of drugs to these sites; and 6) high-dose administration results in significant toxic side effects, including neurotoxicity, ocular toxicity, nephrotoxicity, and ototoxicity, further decreasing patient compliance.[4,5] These challenges have prompted the investigation of an increasing number of second-line anti-TB drugs and their formulations. Rifapentine (RPT), a semisynthetic cyclopentamicin antibiotic, has been approved by the US Food and Drug Administration (FDA) as a first-line anti-TB drug. Its antitubercular mechanism is similar to that of rifampicin, but RPT's minimum inhibitory concentration (MIC) is only 0.12 mg/L to 0.25 mg/L. Its antitubercular activity is 2 to 10 times greater than rifampicin, and its half-life is 4 to 5 times longer, allowing for only 1 to 2 doses per week in clinical practice.[6]

Achieving effective bactericidal concentrations of traditional oral or injectable anti-TB drugs within macrophages remains challenging. This often necessitates the use of high-dose, long-term multidrug combinations to achieve satisfactory therapeutic effects, which increases the risk of adverse reactions and resistance rates and results in poor patient adherence.[7,8] Active targeting of macrophage-specific anti-TB drug delivery systems offers a novel approach to

tuberculosis treatment.[9] This involves modifying drug delivery carriers with specific ligands that bind to phagocytic receptors on macrophages, thereby inducing ligand-receptor interactions to enhance the phagocytosis of drug-loaded systems by macrophages and achieve effective bactericidal concentrations within macrophages.[10,11]

Numerous studies have demonstrated that nanotechnology can significantly enhance the therapeutic efficacy of traditional drugs, attracting widespread attention in the biomedical field.[12,13] To date, various polymeric nanocarriers have been developed and used for targeted drug delivery.[14] With the continuous advancement of nanotechnology, functional groups responsive to different biological microenvironments have been incorporated into the design of novel drug carriers, aiming to improve drug accumulation at disease sites while reducing side effects. Nanodrug carriers have shown tremendous potential in cancer treatment, metabolic disease therapy, and antimicrobial applications.[15–17] Tuberculosis, a chronic infectious disease caused by Mycobacterium tuberculosis, is most commonly manifested as pulmonary tuberculosis. Traditional formulations and administration routes of anti-tuberculosis drugs struggle to maintain effective drug concentrations at the lesion sites, while high-dose combination therapy often leads to significant adverse effects.[13,18] Poor patient adherence and irregular medication further contribute to the emergence of multidrug-resistant strains. As a result, researchers have been searching for more effective treatment methods. The rise of medicine and nanoscience has spurred the development of nanomaterials, and the application of nanomaterials as drug carriers has provided a new direction in medical science. Nanotechnology holds considerable promise in the diagnosis, treatment, and prevention of infectious diseases, including tuberculosis. The main advantages of nanoparticles as drug carriers include their small size, high stability, enhanced delivery of both hydrophilic and hydrophobic drugs, as well as the ability to deliver large molecules into cells.[19] Furthermore, they allow for targeted drug delivery to specific cells or tissues, and offer the feasibility of various administration routes.[20] These carriers also exhibit strong adaptability, ease of control, and slow, sustained drug release from the carrier systems.[21]

Polylactic-co-glycolic acid (PLGA) is a commonly utilized biodegradable polymer, primarily due to its biocompatible metabolites, lactic acid and glycolic acid. These metabolites are soluble in standard solvents and naturally metabolized by the body through the tricarboxylic acid (Krebs) cycle. Furthermore, PLGA can be engineered into diverse shapes and sizes, making it a preferred carrier for delivering drugs, proteins, and macromolecules (eg, DNA, RNA and peptides) to study their physicochemical properties.[22,23] The polymer's properties can be further 'intelligently regulated' by adjusting the ratio of lactic acid to glycolic acid monomers and modifying the physical properties of PLGA nanocarriers, such as size, shape, surface area, and volume, allowing for tailored drug release rates.[24] Due to its excellent biocompatibility and adaptability, PLGA has received approval for a range of biomedical applications and is authorized by the US FDA for human use, particularly in sustained-release drug delivery systems.[25,26] Additionally, polyethylene glycol (PEG) can further provide a steric barrier to prolong the circulation time of nanoparticles (NPs).[22,27]

The macrophage mannose receptor is a transmembrane protein with multiple carbohydrate-binding domains, including a cysteine-rich domain and several C-type lectin domains. These domains can specifically bind to mannose and other carbohydrate molecules, facilitating immune recognition, phagocytosis, and immunomodulation.[28] Based on the above research background, the goal of this study is to synthesize a nanoparticle system capable of loading anti-tuberculosis drugs and investigate its effect on Mycobacterium tuberculosis (Mtb) within macrophages. Currently, isoniazid and rifampicin are still the first-line drugs for tuberculosis treatment, and several drug delivery systems for isoniazid or rifampicin have been reported in the literature.[29–31] In this study, rifapentine was selected as the therapeutic drug in the drug delivery system for the following reasons: 1. Although rifampicin is a first-line anti-tuberculosis drug in the rifamycin-class of antibiotics, around 500,000 new cases of rifampicin-resistant tuberculosis occur each year,[1] which may limit its clinical use. Moreover, the World Health Organization has expressed concern about the low bioavailability of the rifampicin/isoniazid combination therapy.[32] 2. Rifapentine, a derivative of rifamycin, shares a similar structure and activity with rifampicin. Studies have shown that combination therapy based on rifapentine can prevent the emergence of rifampicin-resistant Mtb strains.[33] 3. More importantly, rifapentine has several times the activity against Mtb compared to rifampicin, with a minimum inhibitory concentration (MIC) as low as 0.02–0.06 μg/mL.[34] This characteristic is advantageous for encapsulating the drug in polymers, reducing the required dosage. Additionally, PLGA-PEG was chosen as the nanoparticle carrier in this study. PLGA is one of the most widely used polymers, approved for use in drug delivery systems in the US and Europe, with excellent biocompatibility and the ability to degrade in vivo. More

importantly, it provides opportunities for further structural modifications, especially on the nanoparticle surface, to enhance its therapeutic performance.[35,36] For example, PEG (polyethylene glycol) is a hydrophilic, inert polymer that, when added to nanoparticles, improves their hydrophilicity, facilitates escape from hepatic cell phagocytosis, enhances nanoparticle stability in the body, reduces premature drug release, and prolongs the circulation time in vivo, indirectly increasing the "macrophage targeting" drug quantity in circulation.[37,38] Mannosamine, an amino sugar molecule with an amine group in its structure, can bind efficiently to the mannose receptors on the surface of macrophages. As a result, it has wide applications in macrophage-targeted drug delivery systems.[39] The mannosamine molecules conjugated to the nanoparticle surface enhance the nanoparticles' affinity for macrophages. This ligand-receptor interaction is crucial for targeted drug delivery. Upon binding to the mannose receptor, the receptor-mediated endocytosis process is activated, and the macrophage internalizes the nanoparticles, thereby delivering the drug directly into the cells.[40] Because the drug concentration is significantly increased in the targeted cells, this method can enhance the therapeutic effect without increasing the drug dose. Therefore, we have designed and constructed a mannosamine-modified PLGA-PEG nanoparticle drug delivery system for the targeted delivery of rifapentine to macrophages, aiming to enhance the intracellular killing ability against Mtb.

Materials and Methods

Materials

All chemicals and reagents were obtained from Sigma (USA), unless otherwise specified. Rifapentine (RPT, purity: 98%) was purchased from Solarbio Technology Co., Ltd. (Beijing, China). PLGA-PEG (Mw: 3000)-COOH (Mw: 19,000; lactide ratio: 50:50) was procured from Xi'an Ruixi Biological Technology Co., Ltd. (Shaanxi, China). D-mannosamine was purchased from Merck (USA). Dialysis bags (MWCO: 8000–14,000) were purchased from Shanghai Yuanye Biological Technology Co., Ltd. (Shanghai, China). Dulbecco's Modified Eagle's Medium (DMEM), trypsin-EDTA, fetal bovine serum (FBS), and penicillin-streptomycin solution were obtained from Thermo Fisher Scientific (Waltham, MA, USA). BCG and H37Rv were acquired from ATCC (USA). The Cell Counting Kit-8 (CCK-8) was sourced from AbMole (USA), and the 7H9 medium and OADC supplement were obtained from BD (USA). The RAW264.7 cell line was purchased from Pricella Biotechnology Co., Ltd. (Wuhan, China).

Animals

Male Sprague-Dawley (SD) rats, weighing 180g to 220 g, were used in this study. The rats were housed five per cage under controlled environmental conditions, with room temperature maintained at 25 °C ± 2 °C, humidity at 50% ± 5%, and a 12-hour light/dark cycle. Food and water were provided ad libitum to maintain the rats in a stable physiological state throughout the experimental period.

Preparation of RPT-Loaded NPs

Fifty milligrams of poly(lactic-co-glycolic acid)-polyethylene glycol-carboxyl (PLGA-PEG-COOH) was weighed and transferred into a 50 mL beaker, followed by the addition of 20 mL of dimethyl sulfoxide (DMSO). Once fully dissolved, 50 mg of 1-Ethyl-3-(3-dimethylaminopropyl)carbodiimide hydrochloride (EDC) and 60 mg of N-hydroxysuccinimide (NHS) were weighed and added.[41] Ultrasonication was carried out using an ultrasonic cleaner. The solution was incubated on a shaker at 37°C for 30 minutes. Subsequently, 10 mg of D-mannosamine was added, and the mixture was placed on a shaker.[42] After 24 hours of reaction, the solution was transferred into a dialysis bag. The dialysis bag was placed in a beaker containing pure water, and the magnetic stirrer was activated. After 72 hours of dialysis in pure water, the sample was centrifuged at 4500 rpm. The dialysate was dispensed into a 10 mL white glass bottle and freeze-dried for future use.

Seventy milligrams of D-mannosamine-modified PLGA-PEG (MAN-PLGA-PEG) and 10 mg of rifapentine were dissolved ultrasonically in 2 mL of dichloromethane solution, after which the resulting suspension was added to 15 mL of 0.5% polyvinyl alcohol (PVA) aqueous solution and sonicated in an ice bath (sonication time of 2 seconds at 3-second intervals and 90 W power for 80 cycles). The suspension was transferred into a 50 mL three-necked flask and mechanically stirred at 400 rpm for 4 hours at room temperature to completely volatilize the dichloromethane. Excess

MAN-PLGA-PEG, PVA, and other impurities were removed by washing the nanomaterial three times using ultrafiltration tube centrifugation with a pore size of 10 kDa. The centrifugation was performed at a speed of 4000 rpm to ensure efficient removal of impurities. The nanoparticle was collected, yielding rifapentine-loaded MAN-PLGA-PEG nanoparticles (RPT-MAN-PLGA-PEG NPs). For coumarin 6-labeled nanoparticles used in phagocytic studies, coumarin 6 was added to the dichloromethane, which was the only modification to the procedure described above.

Physicochemical Characterization

The particle size and polydispersity index (PDI) were measured using dynamic light scattering (DLS), while zeta potential was determined by assessing electrophoretic mobility. Each sample was diluted in purified water at 25°C. Measurements were conducted in triplicate using a ZetaSizer Nano-ZS (Malvern Instruments Ltd., Malvern, UK). The product was further analyzed using Fourier transform infrared (FTIR) spectroscopy (Shimadzu, Japan). The spectra of D-mannosamine, PLGA-PEG, and MAN-PLGA-PEG were recorded between wavelengths range of 500 and 4,000 cm^{-1}. Additionally, the conjugates were further characterized using ^{1}H NMR spectroscopy on a Bruker spectrometer, and the morphology was observed by transmission electron Microscopy (TEM, HT-7800, Hitachi, Ltd., Japan). X-ray photoelectron spectroscopy (XPS) analysis was performed using an X-ray photoelectron spectrometer (ESCALAB 250Xi, Thermo Fisher Scientific, USA).

Thermogravimetry Analysis

Thermogravimetric analysis (TGA) was conducted using a TGA, Q600 (TA Instruments, USA) in ramp mode, with a temperature range from 30°C to 600°C at a heating rate of 10°C/min under a nitrogen atmosphere.[43]

Determination of Drug Entrapment Efficiency (EE%) and Drug Loading (DL%)

To determine the drug entrapment efficiency and drug loading, 1 mg of nanoparticles was accurately weighed into a glass test tube, and 1 mL of dichloromethane was added. This was mixed thoroughly and sonicated at 500 W for 10 minutes. The dichloromethane was evaporated under a nitrogen stream at room temperature until completely volatilized. The residue was reconstituted to a final volume of 2 mL with high-performance liquid chromatography (HPLC)-grade methanol. The resulting solution was filtered through a 0.22 μm membrane filter and transferred into an HPLC sample vial. HPLC analysis was conducted using a C18 column (4.6 × 150 mm, 5 μm, Elite, Dalian, China) at a column temperature of 30°C, with a detection wavelength of 335 nm, a flow rate of 1.0 mL/min, and an injection volume of 10 μL. The drug content in the nanoparticles was quantified by analyzing the peak area under the specified chromatographic conditions and applying the results to a standard curve equation. The drug loading (DL%) and encapsulation efficiency (EE%) of the nanoparticles were subsequently calculated using the established equations (Eq1 and Eq2).

$$\mathrm{EE} = \frac{\text{Entrapped drug}}{\text{Drug added}} \times 100 \tag{1}$$

$$\mathrm{DL} = \frac{\text{Entrapped drug}}{\text{Nanoparticle weight}} \times 100 \tag{2}$$

Stability Tests

Freshly prepared freeze-dried NPs were stored in a stability chamber at 25°C for 3 months. At the same time, we freeze-dried the prepared nanomaterial and reconstituted it using medium. Samples were periodically collected to measure particle size, polydispersity index (PDI), and encapsulation efficiency (EE%). The overall stability was assessed by comparing particle size, PDI, and EE% to the initial encapsulated RPT values. Each analysis was performed in triplicate.

Drug Release Studies

Free RPT, RPT-PLGA-PEG, and RPT-MAN-PLGA-PEG nanoparticles were placed in dialysis bags (MWCO: 8000–14,000) and immersed in 50 mL centrifuge tubes containing 40 mL of PBS buffer (pH 4.5 or 7.4) supplemented with 0.2% Tween-80. The tubes were incubated in a thermostatic shaking water bath at 37°C with a rotation speed of

100 rpm. At predetermined intervals, 1 mL of solution was withdrawn and replaced with an equal volume of PBS buffer at the same pH. The RPT concentration in different samples was determined using HPLC under the specified conditions. Cumulative drug release profiles were plotted over time and fitted to various drug release kinetic models.

In vitro Cytotoxicity Assay

RAW264.7 murine macrophages were seeded into 96-well plates at a density of 2×10^4 cells per well. After 24 hours, drug solutions at different concentrations were added to the wells, followed by an additional 24-hour incubation. The final RPT concentrations were set at 0, 5, 10, 25, and 50 μg/mL. Subsequently, 10 μL of CCK-8 reagent was added to each well and incubated at 37 °C in the dark for 2 hours. The optical density (OD) at 450 nm was then measured using a microplate reader. To assess the cytotoxicity of the blank NPs, the same protocol was followed. RAW264.7 cells were treated with blank NPs at various concentrations (0 mg/mL to 1.2 mg/mL). Twelve replicate wells were prepared for each concentration, and PBS buffer was added to the outermost wells of the plate to minimize edge effects.

Cellular Uptake

Flow cytometry was employed to evaluate the uptake of RPT-MAN-PLGA-PEG nanoparticles by RAW264.7 murine macrophages. Log-phase RAW264.7 cells were diluted to a concentration of 1×10^6 cells/mL and seeded into six-well plates. The cells were treated with Coumarin-6 fluorescently labeled PLGA-PEG, MAN-PLGA-PEG, RPT-PLGA-PEG, and RPT-MAN-PLGA-PEG NPs for 0.5, 1, 3, 6, 12 and 24 hours.[44] Untreated RAW264.7 cells served as the negative control group. After incubation, the cells were gently washed with PBS to remove nanoparticles adhering to the cell membrane and not internalized. The cells were then collected, centrifuged at 1000 rpm for 5 minutes, and resuspended in PBS. In a parallel experiment, 0.05 M D-mannosamine was added to assess the effect of mannose receptor inhibition on the uptake of MAN-PLGA-PEG and RPT-MAN-PLGA-PEG nanoparticles by macrophages. All other steps were performed as described above. Data analysis was performed using FlowJo version 10 (FlowJo LLC, Ashland, OR, USA).

For confocal imaging, RAW264.7 cells were seeded into laser confocal dishes at a density of 5×10^4 cells/mL and cultured for 24 hours to ensure uniform cell density across groups. Coumarin-6-labeled PLGA-PEG NPs and MAN-PLGA-PEG NPs were suspended in the culture medium and added to the dishes, with untreated cells serving as a negative control. After co-incubation for 6 hours, the cells were washed three times with PBS to remove residual NPs adhering to the cell membrane. The cells were then fixed with 4% paraformaldehyde and stained with 5 μg/mL DAPI for 15 minutes to visualize the nuclear morphology. Images were captured using a confocal laser scanning microscope (Leica, Germany), where coumarin-6 and DAPI emitted green and blue fluorescence, respectively.

Haemolytic Toxicity

The hemolysis rate was used to evaluate the compatibility of NPs with red blood cells. Blood samples were collected from SD rats and centrifuged at 3000 rpm for 20 minutes to separate the red blood cells, which were subsequently resuspended in 0.9% w/v saline. NPs at varying concentrations (0.5, 1.5 and 3.5 mg/mL) were prepared in normal saline and incubated with the red blood cell suspension.[41] The collected red blood cell suspensions were first subjected to a full-spectrum UV spectrophotometric scan across the wavelength range of 200–800 nm to identify and record the absorption peaks. Based on the measurements, wavelengths of 541.5 nm and 576.5 nm were selected. Additionally, 545 nm,[45] a wavelength commonly cited in the literature, was included in our analysis to enhance the robustness of the results. Distilled water was used as the positive control. Absorbance was measured at 541.5 nm, 545 nm, and 576.5 nm using a UV-visible spectrophotometer. The hemolytic rate of each sample was calculated using the formula: Haemolytic rate (%) = [(Absorbance of sample − Absorbance of saline)/(Absorbance of water − Absorbance of saline)] × 100.

In vitro Anti-Tubercular Studies

The antimycobacterial activity of NPs against Mycobacterium tuberculosis was evaluated using a microplate Alamar Blue assay following a previously established protocol.[45,46] The Mycobacterium tuberculosis H37Rv strain was cultured in modified Löwenstein-Jensen medium and incubated at 37°C for 2–3 weeks. To prepare the bacterial suspension, 1–2 drops of 5% Tween-80 were added to a sterile grinding bottle. Fresh bacterial colonies were carefully scraped from the culture medium using

a sterile inoculation loop and transferred into the bottle. The suspension was then vortexed for 20 seconds and allowed to settle. Following this, 2 mL of physiological saline was added, thoroughly mixed, and allowed to settle again. The supernatant was carefully collected using a sterile pipette and adjusted to a turbidity equivalent to 1 McFarland standard. Finally, dilute the bacterial suspension with 7H9 liquid medium supplemented with OADC to prepare for subsequent experiments. First, 200 μL of sterile deionized water was added to the outer peripheral wells to prevent evaporation. Next, 100 μL of either free rifapentine or rifapentine-loaded nanoparticle formulations was added to each well. Serial 1:2 dilutions were then performed in columns 3 through 10. The final concentration range for free RPT was set between 1.6 μg/mL and 0.006 μg/mL and between 0.75 μg/mL and 0.003 μg/mL for drug-loaded NPs. Finally, 100 μL of the previously diluted Mycobacterium tuberculosis inoculum was added to wells in columns 2 through 11. Column 11 served as the positive control without drug. After 7 days of incubation, 50 μL of Alamar Blue reagent was added, followed by re-incubation for an additional 24 hours. The results were analyzed based on color changes in each well. The concentration corresponding to no observable bacterial growth was recorded as the minimum inhibitory concentration of the formulation.

Intracellular Inhibition of Mycobacterium Tuberculosis by NPs

The colony-forming unit(CFU)assay was used to evaluate the bactericidal effects of nanoparticles on Mycobacterium tuberculosis(MTB)in RAW264.7 cells infected with MTB. Free drugs at a concentration of 0.047 μg/mL and nanoparticles containing an equivalent drug concentration were used for the intervention. RAW264.7 cells were seeded at a density of 1×10^6 cells per well in 12-well plates and infected with BCG at a MOI of 1 for 24 hours or H37Rv at a MOI of 1 for 4 hours. The cells were then incubated with the drugs or nanoparticles for 72 hours. After incubation, the cells were washed three times with PBS, lysed with PBS containing 0.03% SDS for 10 minutes to release intracellular MTB, and the lysates were collected. Each group included three replicates. The lysates were serially diluted in 7H9 medium, plated on Middlebrook 7H11 plates, and incubated at 37°C for 21 days to quantify CFUs.

Pharmacokinetics Study

This animal experiment was approved by the Animal Ethics Committee of Xinjiang Medical University (Approval No. 20240711–18). The study was conducted in accordance with the principles and guidelines approved by the committee, as well as the NIH Guide for the Care and Use of Laboratory Animals (Eighth Edition) and internationally recognized guidelines.[47] Male Sprague-Dawley (SD) rats weighing 180g to 220g were randomly divided into three groups: free rifapentine, RPT-PLGA-PEG, and RPT-MAN-PLGA-PEG nanoparticles. SD rats were intraperitoneally injected with 2% sodium pentobarbital (3mg/100g) for anesthesia. Each rat received a single intravenous injection of the drug or nanoparticles with equal drug content (10 mg/kg) at the same time. Blood samples were collected from the rats at predetermined time points via orbital bleeding. Proteins were separated from plasma using acetonitrile, and supernatants were collected by centrifugation.[48] The concentration of RPT in plasma was measured using HPLC. The maximum concentration (C_{max}), time to reach maximum plasma concentration (T_{max}), half-life ($t_{1/2}$), mean residence time (MRT), and area under the curve ($AUC_{0-\infty}$) were evaluated.

Tissue Distribution Studies

In a single-dose rifapentine disposition study, mice in each group received a single intravenous dose of 10 mg/kg rifapentine. The mice were divided into four groups: control (normal saline), rifapentine, RPT-PLGA-PEG NPs, and RPT-MAN-PLGA-PEG NPs. The animals were sacrificed at specified time intervals. After plasma collection, tissues (liver, kidneys, and lungs) were excised, quickly washed with normal saline, and stored at −80°C. Drug concentrations were estimated in 20% (w/v) tissue homogenates. Rifapentine content was measured using the HPLC method as described previously. The results were expressed as μg/g (microgram per gram of tissue).

To evaluate the potential toxicity of NPs in different organs, animals were euthanized on the fourth day after injection. The heart, kidneys, liver, lungs, and spleen were excised and immediately rinsed with saline to remove residual blood. The organs were then immersed in 4% paraformaldehyde solution in centrifuge tubes for 72 hours for tissue fixation. Fixed tissues were embedded in paraffin and stained with hematoxylin and eosin (H&E) to assess any pathological changes in the organs. Biochemical analyses were performed on collected blood samples to evaluate potential hepatic and renal function impairments through standard biochemical tests.

Statistical Analysis

All experiments were conducted in triplicate, with each experiment repeated at least three times. Results are expressed as the mean ± standard deviation (SD). Statistical analyses were conducted using SPSS version 17.0 software. One-way analysis of variance (ANOVA) followed by Tukey's post-hoc test was used for group comparisons. A P-value of <0.05 was considered statistically significant.

Results and Discussion

Physicochemical Characterization

The ^{1}H NMR spectra of D-mannosamine, PLGA-PEG-COOH, and MAN-PLGA-PEG were analyzed, as displayed in Figure 1A. In the ^{1}H NMR spectrum of PLGA-PEG-COOH, the peak at 8.13 ppm represents the characteristic signal of the -OH group in the carboxylic acid. Peaks at 1.48 ppm and 5.21 ppm correspond to the characteristic signals of the methyl and methine groups of the glycolic acid (GA) segment, respectively, while the peak at 4.91 ppm corresponds to the methylene group of the lactic acid (LA) segment. In the ^{1}H NMR spectrum of D-mannosamine, peaks at 5.24 and 5.05 ppm correspond to terminal hydrogen atoms, while peaks between 3.54 and 3.41 ppm correspond to methylene protons, and those between 4.05 and 3.77 ppm correspond to methine protons. In the ^{1}H NMR spectrum of MAN-PLGA-PEG, Peaks at 1.48 and 5.20 ppm represent the methyl and methine groups of the glycolic acid (GA) segment, while the peak at 4.91 ppm corresponds to the methylene group of the lactic acid (LA) segment, all of which belong to the PLGA chain. The peak at 3.51 ppm is assigned to the methylene group of the PEG segment. The integration ratio of the characteristic peaks of the PEG and PLGA chains suggests an approximate molar ratio of 1:1 between PEG and PLGA. A comparison of the ^{1}H NMR spectra of D-mannosamine, PLGA-PEG-COOH, and MAN-PLGA-PEG reveals a distinct

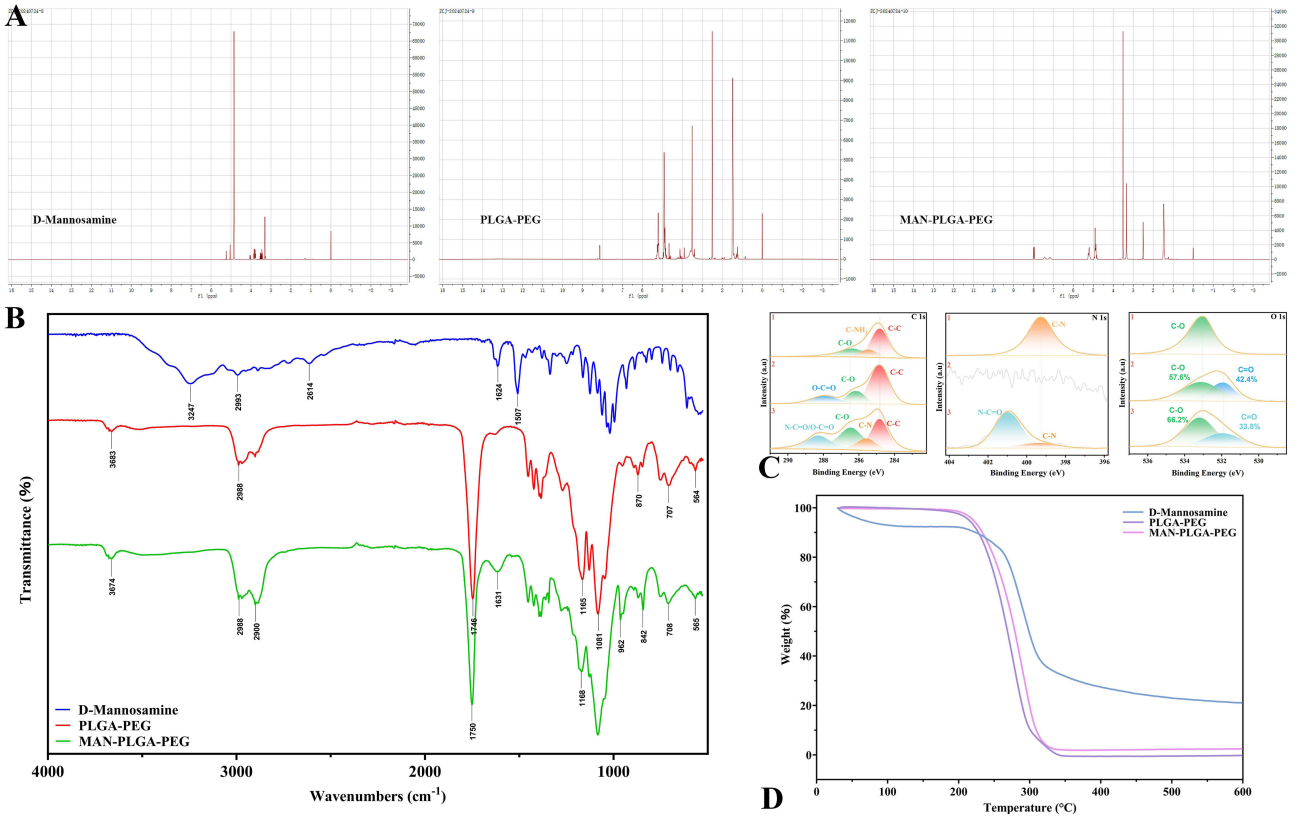

Figure 1 Physicochemical characterization of the nanomaterials. (**A**) Proton nuclear magnetic resonance (^{1}H NMR) spectra. (**B**) Fourier transform infrared (FTIR) spectra of D-mannosamine, PLGA-PEG-COOH, and MAN-PLGA-PEG. (**C**) X-ray photoelectron spectroscopy (XPS) results of the same materials, with 1 representing D-mannosamine, 2 representing PLGA-PEG-COOH, and 3 representing MAN-PLGA-PEG and (**D**) thermogravimetric analysis (TGA) of the three materials.

 https://doi.org/10.2147/DDDT.S505682

peak at 7.5 ppm in the MAN-PLGA-PEG spectrum, which is attributed to the formation of an amide bond, thereby confirming the successful conjugation of D-mannosamine to PLGA-PEG-COOH.

Fourier transform infrared (FTIR) spectroscopy was conducted on MAN-PLGA-PEG to confirm the conjugation of D-mannosamine onto the surface of PLGA-PEG, and the results are presented in the Figure 1B. The absorption bands in the 3300cm^{-1} to 2800 cm^{-1} region correspond to the stretching vibrations of C-H bonds. Absorption at wavelengths above 3000 cm^{-1} corresponds to the stretching vibrations of unsaturated C-H bonds, whereas absorption below 3000 cm^{-1} generally corresponds to the stretching vibrations of saturated C-H bonds. The absorption bands around 2960cm^{-1} to 2850 cm^{-1} are typically associated with the stretching vibrations of methyl, methylene, and methine groups in alkanes.[39] The absorption band near 1750 cm^{-1} represents the characteristic peak of carbonyl (C=O) functional groups, which are formed by a double bond between carbon and oxygen. The absorption band around 1650 cm^{-1} corresponds to the amide I band, primarily attributed to C=O stretching vibrations, representing the strongest absorption peak of the amide bond. The absorption bands between 1450cm^{-1} to 1300 cm^{-1} are mainly associated with the stretching vibrations of saturated hydrocarbon C-H bonds, whereas the absorption band near 1290 cm^{-1} corresponds to the amide III band, primarily due to C-N stretching vibrations. The absorption region between 1000cm^{-1} to 1250 cm^{-1} is primarily attributed to the stretching vibrations of C-O and C-O-C bonds. In summary, the FTIR spectrum of MAN-PLGA-PEG showed prominent stretching vibration peaks for C=O and C-O bonds, along with characteristic absorption peaks for amides, particularly the amide I and amide III bands. These spectral features confirm that the amide bond formation between the activated carboxyl groups of PLGA-PEG and the amino groups of D-mannosamine had occurred, thereby validating the successful conjugation of D-mannosamine onto PLGA-PEG.

To elucidate the internal composition of the three materials and confirm that D-mannosamine and PLGA-PEG-COOH undergo dehydration condensation reactions to form amide bonds, X-ray photoelectron spectroscopy (XPS) was conducted. Figure 1C presents the high-resolution C 1s spectra of D-mannosamine, PLGA-PEG-COOH, and MAN-PLGA-PEG. The three peaks in the D-mannosamine spectrum correspond to C-C, C-NH2, and C-O bonds, respectively, while the PLGA-PEG-COOH spectrum exhibits a peak around 288 eV, indicating aldehyde groups. Notably, C-N and C-O bonds are observed in MAN-PLGA-PEG, with shifts to higher binding energies compared to mannosamine and PLGA-PEG-COOH, attributed to changes in the bonding environment after the polymerization of -NH_2 in mannosamine and -OH in PLGA-PEG-COOH, leading to increased binding energy. Additionally, the peak at 288.4 eV is attributed to a complex peak representing both the amide bond and aldehyde group, which results in a shift from the original aldehyde peak at 288 eV. In the high-resolution N 1s spectra, the only significant peak in D-mannosamine corresponds to C-N bonding, while no nitrogen was detected in PLGA-PEG-COOH, consistent with its internal structural composition. The N 1s spectrum of MAN-PLGA-PEG displayed a significant decrease in the C-N bonding ratio at 399.7 eV, along with the appearance of a new peak at 401 eV corresponding to N-C=O, further confirming that D-mannosamine and PLGA-PEG-COOH underwent dehydration condensation to form MAN-PLGA-PEG. In MAN-PLGA-PEG, compared to PLGA-PEG-COOH, the C-O bonding ratio (66.2) was higher than in PLGA-PEG-COOH (57.6). This increase is attributed to the polymerization of D-mannosamine during the conjugation process, which is consistent with the formation of the amide bond between D-mannosamine and PLGA-PEG-COOH, providing further evidence of the successful conjugation.

Thermogravimetric analysis (TGA) was conducted for D-mannosamine, PLGA-PEG-COOH, and MAN-PLGA-PEG over a temperature range of 30 °C to 600°C, as shown in Figure 1D. D-mannosamine exhibited two stages of mass loss. In the first stage, a 7.58% w/w weight loss between 30 °C and 123.18 °C was attributed to the desorption of adsorbed and bound water, a typical behavior for hydrophilic compounds. In the second weight loss stage, a more notable mass loss of 55.63% w/w was observed between 265.88 °C and 450.83 °C. This weight loss was associated with the decomposition of D-mannosamine, likely involving the breakdown of its organic structure under thermal conditions. The PLGA-PEG-COOH and MAN-PLGA-PEG copolymers displayed a single stage of mass loss around 230.87 °C and 238.38 °C, respectively. Furthermore, the incorporation of D-mannosamine into the PLGA-PEG-COOH matrix enhanced the thermal stability of MAN-PLGA-PEG compared to the unmodified PLGA-PEG-COOH. This improvement in thermal stability is likely due to the formation of strong amide bonds between the D-mannosamine and PLGA-PEG-COOH, which contribute to a more robust polymer structure that is more resistant to thermal degradation.[43,49,50]

Table 1 Physicochemical Characterization of Rifapentine Loaded NPs

	Size	ZP (mv)	PDI	EE (%)	DL (%)
PLGA-PEG	106.3±8.5	−19.89±0.31	0.184±0.016	–	–
MAN-PLGA-PEG	106.9±9.2	−16.37±0.43	0.178±0.029	–	–
RPT-PLGA-PEG	107.1±6.7	−20.54±0.84	0.172±0.018	79.5±5.7	13.2±0.4
RPT-MAN-PLGA-PEG	108.2±7.2	−15.35±0.77	0.190±0.015	81.2±6.3	13.7±0.7

Abbreviations: RPT, rifapentine; MAN, Mannosamine; PLGA, poly-d,l-lactide-co-glycolide; PEG, poly ethylene glycol; PDI, polydispersity index; ZP, zeta potential; EE, encapsulation efficiency; DL, drug loading.

Particle size plays a critical role in determining the specific physicochemical properties of NPs; thus, accurate measurement of particle size is essential for drug delivery systems.[51,52] The size of NPs significantly influences their biodistribution, cellular uptake, and clearance from the body. Typically, NPs with sizes below 10 nm are cleared through the kidneys via renal filtration,[53,54] while those above 200 nm tend to have faster plasma clearance rates.[55] In this study, the RPT-MAN-PLGA-PEG NPs had an average size of 108.2 ± 7.2 nm (Table 1 and Figure 2A), which is considered suitable for long-term sustained-release delivery. Liu et al[56] reported that NPs of this size can be efficiently phagocytosed by cells and are also large enough to be retained in systemic circulation for extended periods. Ideally, the modification with D-mannosamine should result in significant differences in particle size. However, the absence of significant differences suggests that certain factors may have influenced the outcome. Possible reasons for this lack of difference include: 1) The two types of nanoparticles may possess similar physicochemical properties, such as surface charge, hydrophilicity, and hydrophobicity, which partially determine their stability and particle size. Due to the characteristics of

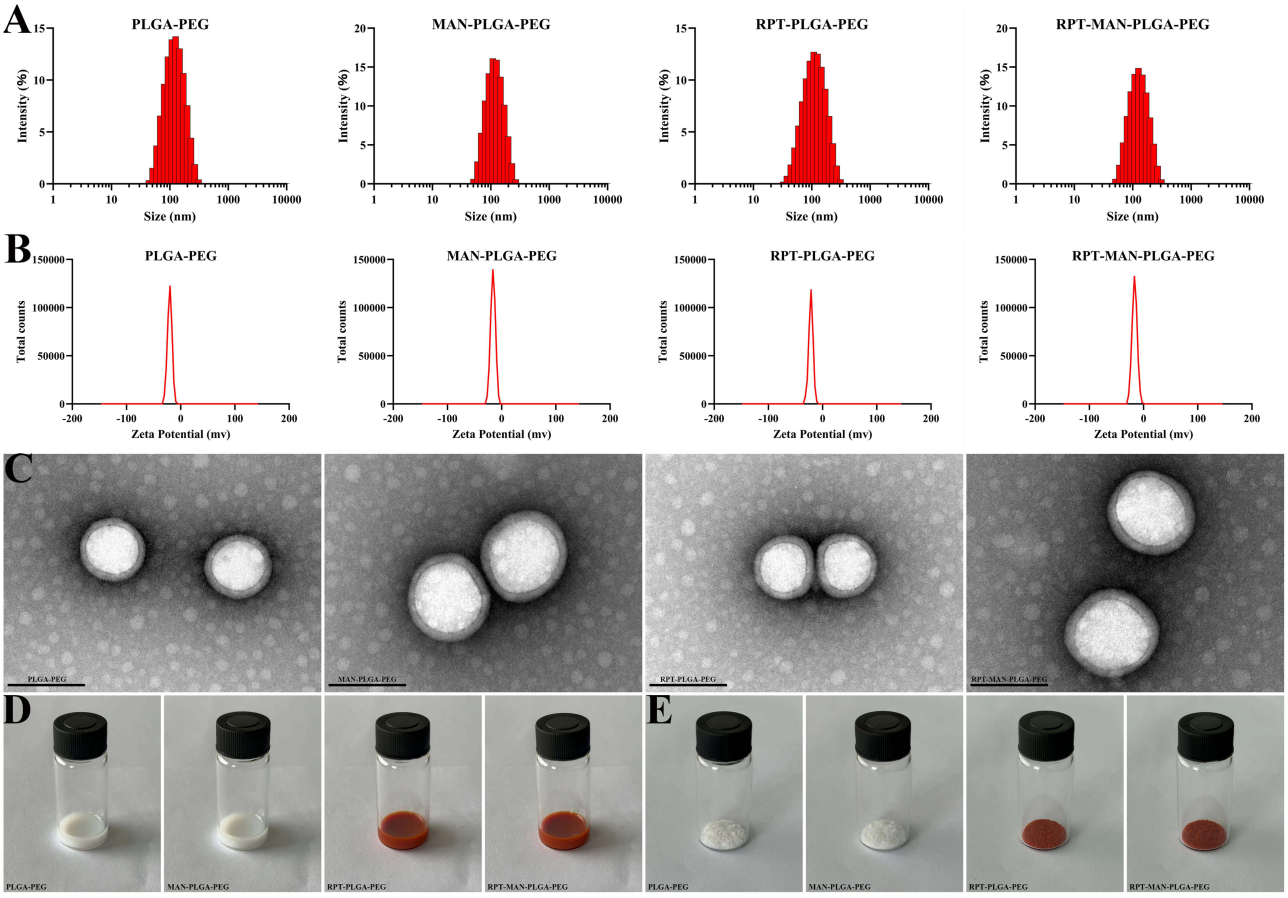

Figure 2 Morphological characterization of the nanomaterials. (**A**) Particle size distribution. (**B**) Zeta potential measurement. (**C**) Transmission electron microscopy (TEM) image of the nanomaterials, scale bar: 100 nm. (**D**) Nanomaterials in liquid state. (**E**) Nanomaterials after lyophilization.

 https://doi.org/10.2147/DDDT.S505682

PLGA (polylactic-co-glycolic acid) and PEG (polyethylene glycol), the overall particle size of nanoparticles may be more significantly influenced by these materials, while the effect of D-mannosamine modification is relatively minor. These properties may thus obscure any influence of D-mannosamine on particle size; 2) Specific modifications to nanodrug delivery systems, such as surface ligand functionalization, are typically designed to enhance targeting efficiency or improve cellular uptake rather than significantly alter particle size. D-mannosamine modification primarily aims to target specific receptors, such as mannose receptors on the surface of macrophages; therefore, it is more likely to affect the targeting capability and cellular uptake of nanoparticles rather than their particle size; 3) Interactions between D-mannosamine, PLGA, and PEG may reduce the potential influence of D-mannosamine on particle size. The presence of PLGA and PEG may partially mask or counteract the impact of D-mannosamine on particle size, thereby maintaining a relatively stable particle size. Therefore, further investigation and exploration of these factors are necessary to better understand the lack of significant differences in particle size.

Positively charged nanoformulations exhibit higher plasma clearance rates compared to their neutral and negatively charged counterparts. Furthermore, the presence of negatively charged serum proteins may promote aggregation following the administration of positively charged nanoparticles, potentially resulting in capillary embolization.[57,58] Moreover, a highly negative surface charge indicates strong electrostatic repulsion between nanoparticles, serving as a critical indicator of stability.[45] Haggag et al[59] reported that PLGA nanoparticles (NPs) exhibited a negative zeta potential, which was significantly greater than that of PEGylated PLGA nanoparticles. In our study, all four types of nanoparticles exhibited negative zeta potentials, The zeta potentials of PLGA-PEG, MAN-PLGA-PEG, RPT-PLGA-PEG and RPT-MAN-PLGA-PEG nanoparticles were −19.89 ± 0.31, −16.37 ± 0.43, −20.54 ± 0.84 and −15.35 ± 0.77, respectively (Table 1 and Figure 2B), primarily attributed to the presence of carboxyl groups at the termini of the PLGA chains. The slight decrease in the zeta potential of MAN-PLGA-PEG NPs may be attributed to D-mannosamine, which contains both an amino group (-NH_2) and a hydroxyl group (-OH). In neutral or mildly basic environments, the amino group may become partially protonated (positively charged), resulting in a neutralizing effect on the overall surface potential. However, the concentration of D-mannosamine is insufficient to fully neutralize the negative charge on the PLGA-PEG surface.

Transmission electron microscopy (TEM) revealed that all four types of nanoparticles were uniformly dispersed as individual particles with smooth, spherical surfaces. No significant alterations were detected on the surface or within the internal structure of the nanoparticles. High-magnification imaging revealed a core-shell structure, with the core encapsulated by an outer layer, indicating that the drug was embedded within the polymer matrix[60,61] (Figure 2C). The polydispersity coefficients (PDI) of the four nanomaterials were less than 0.2, and the PDI of the four nanomaterials PLGA-PEG, MAN-PLGA-PEG, RPT-PLGA-PEG and RPT-MAN-PLGA-PEG were 0.184 ± 0.016, 0.178 ± 0.029, 0.172 ± 0.018, and 0.190 ± 0.015, respectively, suggesting that the nanoparticles had uniform size, and were less prone to large particles or aggregates, with high kinetic stability (Table 1). Moreover, stability studies indicated no significant variations in particle size, PDI, or encapsulation efficiency, suggesting that both nanoparticle types maintained stability for at least 3 months (Table 2). Figure 2D and E illustrate the morphology of the nanoparticles in their liquid state and after lyophilization, respectively. The liquid formulations of the two drug-loaded NPs appeared brick-red, indicating the presence of the drug (likely due to the color of the rifapentine). These formulations exhibited good fluidity and were free from particles or precipitates, with a smooth texture, suggesting the absence of aggregation or instability in the formulation. To further investigate the effect of RPT on PLGA-PEG NPs, the same preparation method and batch were used to produce non-drug-loaded PLGA-PEG and MAN-PLGA-PEG NPs. The liquid formulations of both these non-drug-loaded NPs appeared milky white, smooth in texture, free of particles or precipitates, and formed a semi-transparent liquid. All four lyophilized nanoparticle formulations were characterized by a loose powder form, with no clumping, particle adhesion, or static adsorption, and demonstrated stable physical properties, further confirming the stability of the NPs. For freeze-dried nanomaterials, no significant changes in physicochemical properties were observed after reconstitution with culture medium (Table 3).

Currently, various nanocarriers loaded with anti-tuberculosis (anti-TB) drugs have been reported, including liposomes, polymeric micelles, and exosomes.[32] However, research on RPT nanoformulations remains limited. Recently, Magalhães et al[62] reported RPT-loaded lipid nanoparticles with a particle size of 242 nm, a polydispersity index (PDI) of 0.17, a zeta potential (ZP) of −22 mV, an encapsulation efficiency (EE%) of 86%, and a drug loading (DL%) of 2.9%. In

Table 2 Stability Evaluation Within Three Months

	Time	Size (nm)	PDI	EE (%)
RPT-PLGA-PEG	Initial	107.1±6.7	0.17±0.02	79.5±5.7
	1 month	107.8±4.9	0.17±0.03	78.3±6.8
	2 months	108.5±5.4	0.18±0.07	77.5±5.4
	3 months	108.9±6.3	0.19±0.05	77.1±8.1
RPT-MAN-PLGA-PEG	Initial	108.2±7.2	0.19±0.02	81.2±6.3
	1 month	108.9±7.9	0.20±0.03	80.3±7.3
	2 months	109.3±8.3	0.20±0.04	79.9±4.1
	3 months	109.6±5.2	0.21±0.03	79.2±5.5

Abbreviations: RPT, rifapentine; MAN, Mannosamine; PLGA, poly-d,l-lactide-co-glycolide; PEG, poly ethylene glycol; PDI, polydispersity index; EE, encapsulation efficiency.

Table 3 Physicochemical Characterization of Four Nanomaterials After Freeze Drying and Reconstitution

	Size	PDI	EE (%)
RPT-PLGA-PEG	106.3±4.2	0.181±0.021	77.2±3.6
RPT-MAN-PLGA-PEG	106.7±6.5	0.179±0.037	80.9±5.2

Abbreviations: RPT, rifapentine; MAN, Mannosamine; PLGA, poly-d,l-lactide-co-glycolide; PEG, poly ethylene glycol; PDI, polydispersity index; EE, encapsulation efficiency.

this study, the encapsulation efficiency (EE%) of RPT-MAN-PLGA-PEG NPs was 81.2 ± 6.3%, and the drug loading (DL%) was 13.7 ± 0.7% (Table 1). In comparison, our study's results appear superior in certain aspects of the aforementioned characteristics. The higher drug loading in the current study suggests that a larger amount of rifapentine is effectively encapsulated in the RPT-MAN-PLGA-PEG NPs, which is important for enhancing the antibacterial efficacy and achieving sustained drug release. Smaller particle sizes are generally considered more favorable for extending systemic circulation time. A lower PDI and a more negative zeta potential suggest improved uniformity and stability of the nanoparticles. Higher EE% and DL% may enhance the antibacterial efficacy. In earlier studies, numerous anti-TB drugs-loaded nanoformulations have been reported, particularly those involving rifampicin, the most commonly encapsulated drug.[51,63–65] The particle size, PDI, ZP, EE%, and DL% varied among these formulations, primarily due to differences in the materials and methods used in their preparation. Compared to these studies, the nanoparticles in our research demonstrated a smaller particle size, lower PDI, and higher zeta potential and EE%, which may be attributed to the combined method employed and the inherent properties of RPT.

Haemolytic Toxicity

Assessing the hemolysis rate is essential for evaluating the hemocompatibility of biomaterials, and a low hemolysis rate is indicative of good biocompatibility and safety for in vivo applications.[66] The hemolysis rates of the four nanomaterials developed in this study remained below 5% (Figure 3A–C). This value is well below the generally accepted threshold for hemolysis in biomedical materials, indicating that the RPT-MAN-PLGA-PEG NPs do not induce significant damage to red blood cells and are suitable for systemic administration through blood circulation.[67]

Drug Release Study

Controlled drug release is a key advantage of nanostructured delivery systems over free drugs, enabling selective release at the specific disease site or within targeted cellular organelles, thereby improving drug efficacy and reducing toxicity.[68] The drug release behavior of RPT-MAN-PLGA-PEG NPs was evaluated under simulated blood circulation conditions in PBS at pH 7.4 and simulated lysosomal conditions in PBS at pH 4.5.[69,70] As illustrated in Figure 3D and E, the cumulative release of RPT from RPT-MAN-PLGA-PEG NPs was 11.44% at 3 hours and 54.95% at 48 hours at pH 7.4, while at pH 4.5, it reached approximately 18.44% at 3 hours and 74.95% at 48 hours. These results indicate that acidic conditions enhance the

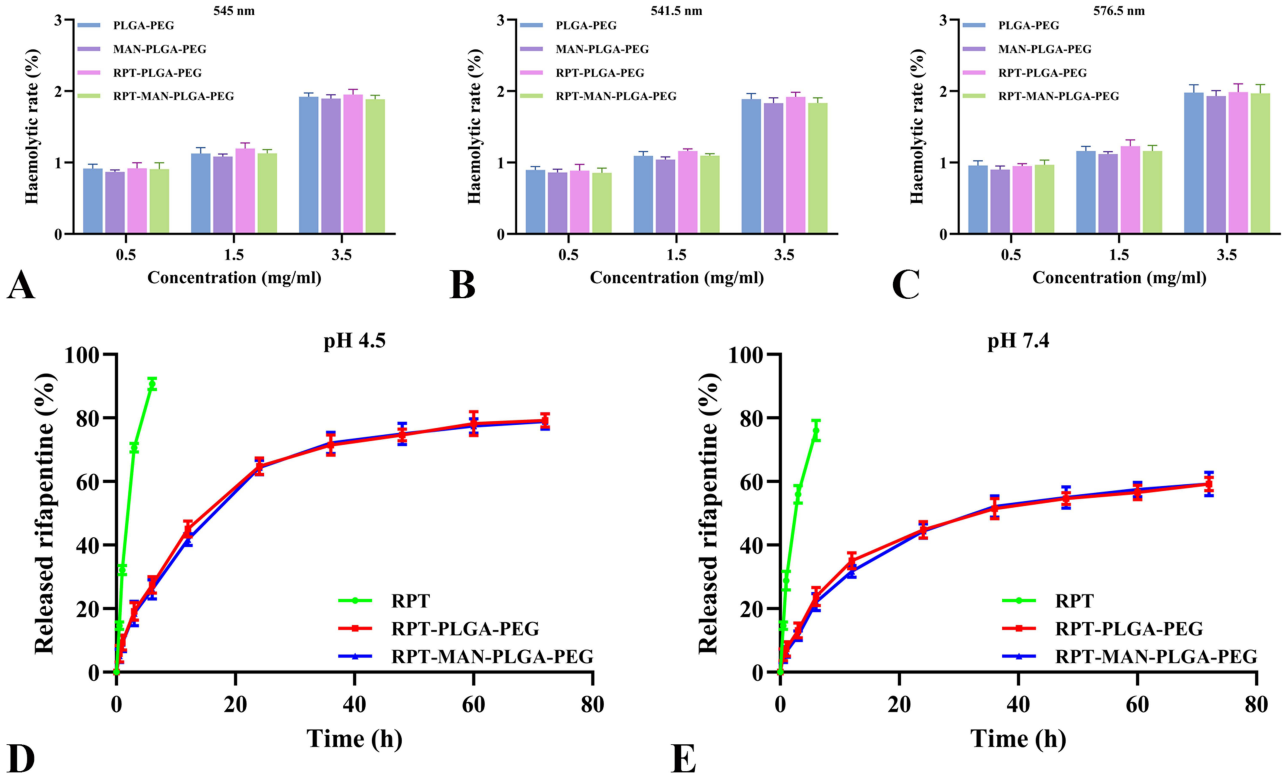

Figure 3 (**A–C**) Hemolysis rates of the nanomaterials at three different wavelengths. (**D**) In vitro release profiles of rifapentine (RPT), RPT-PLGA-PEG, and RPT-MAN-PLGA -PEG NPs at pH 4.5. (**E**) In vitro release profiles of rifapentine (RPT), RPT-PLGA-PEG, and RPT-MAN-PLGA-PEG NPs at pH 7.4, n=9.

release of RPT from RPT-MAN-PLGA-PEG NPs. As MAN-PLGA-PEG were mainly transported into the acidic lysosomes of macrophages, RPT-MAN-PLGA-PEG NPs would accelerate RPT release after their entry of lysosomes and initiate more effective killing of intracellular Mtb. In contrast, free RPT exhibited an initial burst release, with approximately 90.73% released within 9 hours. Overall, the ability to maintain therapeutic concentrations over extended periods makes this controlled release profile ideal for tuberculosis treatment, reducing dosing frequency and minimizing adverse effects. The regression coefficients (R^2) were analyzed by fitting the drug release data to four kinetic models: Zero-order, First-order, Higuchi, and Hixson-Crowell (Table 4). The results demonstrate that the Higuchi model is the most suitable, as it yielded higher R^2 values under both pH conditions (0.9785 and 0.9703 for RPT-PLGA-PEG NPs; 0.9773 and 0.9793 for RPT-MAN -PLGA-PEG NPs). This mathematical model proposes that the drug release rate is proportional to the square root of time.[71,72]

Table 4 Results of the Kinetic Parameters of the Drug Release Profile Obtained for RPT-PLGA-PEG and RPT-MAN-PLGA-PEG NPs: Determination Coefficient (R^2)

	pH	Release model			
		Zero-order	First-order	Higuchi	Hixson-Crowell
RPT-PLGA-PEG	7.4	0.8680	0.8037	0.9785	0.9739
	4.5	0.8399	0.7689	0.9703	0.9661
RPT-MAN-PLGA-PEG	7.4	0.8631	0.8105	0.9773	0.9627
	4.5	0.8463	0.7769	0.9793	0.9682

https://doi.org/10.2147/DDDT.S505682

In vitro Cytotoxicity Assay

The cytotoxicity of both drug-loaded NPs and free RPT was assessed by evaluating cell viability in RAW264.7 macrophage cells. The results indicate that both drug-loaded NPs exhibited no cytotoxicity towards macrophages, as cell viability remained above 80% across all tested concentrations (Figure 4A). In contrast, free RPT at a concentration of 50 μg/mL resulted in a significant decrease in cell viability, which dropped below 60%, suggesting that the nanoformulation may help reduce the inherent cytotoxicity of RPT, improving its biocompatibility. To further evaluate the effect of the blank NPs (NPs without the drug) on cell viability, RAW264.7 cells were co-cultured with various concentrations of blank NPs for 24 hours. The results showed that, at a concentration of 0.6 mg/mL, the cell viability remained above 90%, indicating that blank NPs did not induce significant cytotoxicity at this concentration. However, higher concentrations

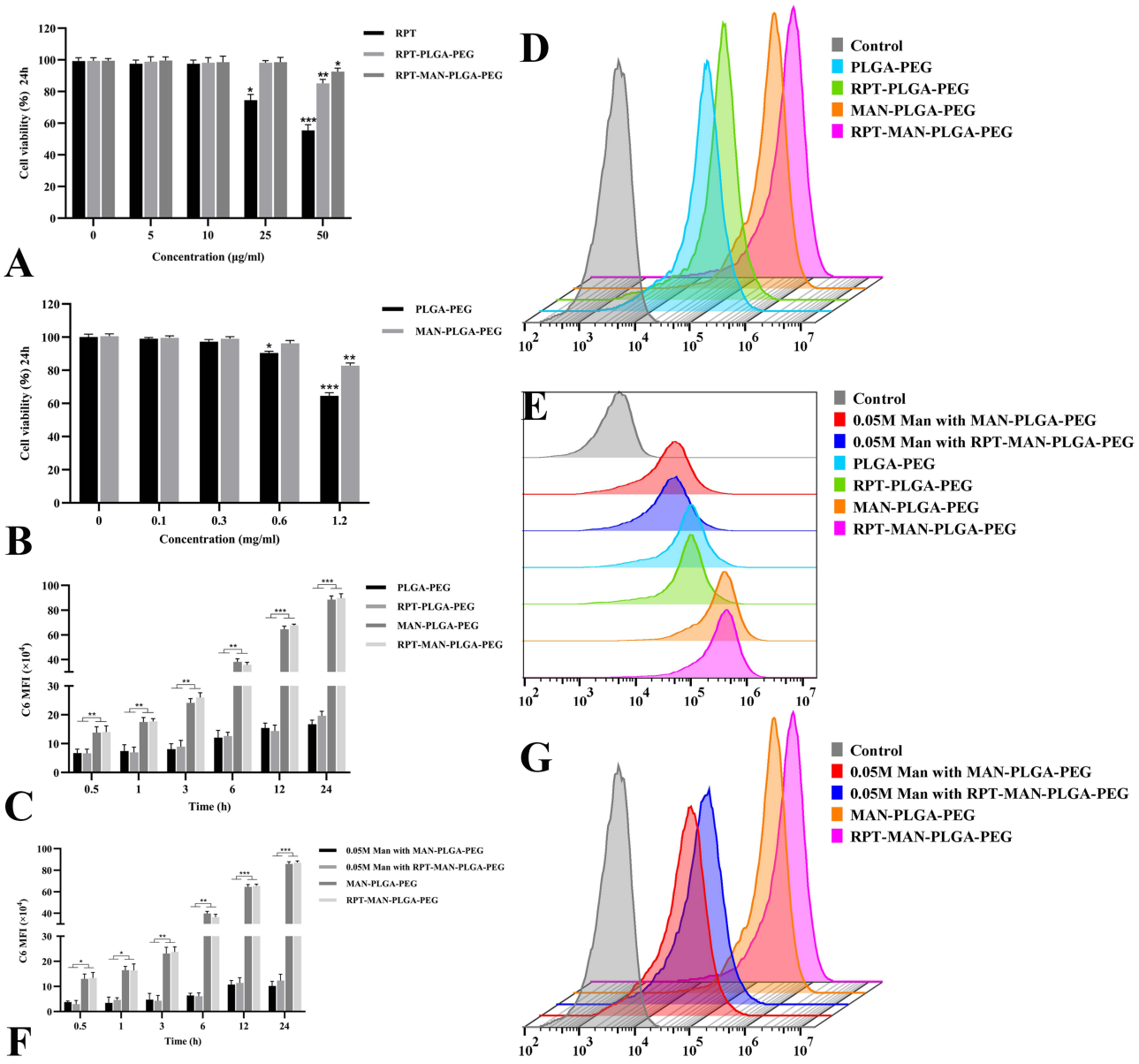

Figure 4 Cytotoxicity and targeting evaluation of nanomaterials in macrophages. (**A**) Cytotoxicity assessment of free rifapentine (RPT), RPT-PLGA-PEG, and RPT-MAN-PLGA-PEG nanoparticles (NPs) in macrophages, *P < 0.05, **P < 0.01, ***P < 0.001. (**B**) Cytotoxicity of blank nanoparticles in macrophages, *P < 0.05, **P < 0.01, ***P < 0.001. (**C**) Time-dependent mean fluorescence intensity (MFI) of different nanoparticles phagocytosed by macrophages, **P < 0.01, ***P < 0.001. (**D, E**) Histograms of fluorescence shift in macrophages after 6 hours of incubation with coumarin-6-labeled nanoparticles at a drug concentration of 5.0 μg/mL, n=9. (**F**) Time-dependent MFI of MAN-PLGA-PEG and RPT-MAN-PLGA-PEG nanoparticles in the presence of D-mannosamine, *P < 0.05, **P < 0.01, ***P < 0.001. (**G**) A fluorescence shift histogram of macrophages incubated with coumarin-6-labeled nanoparticles at a drug concentration of 5.0 μg/mL (n=9) for 6 hours, in the presence of D-mannosamine.

(1.2 mg/mL) of NPs led to a reduction in cell viability, although this effect was not as pronounced as with free RPT (Figure 4B). Importantly, the concentration of NPs used in practical applications is considerably lower than this concentration (1.2 mg/mL).

In vitro Cellular Uptake of Macrophage-Targeted Nanoparticles

The active targeting drug delivery system involves ligand-receptor interactions between the nanoparticle carrier and target cells or tissues. These ligands are typically conjugated to the surface of the drug delivery system, where they are recognized by pattern recognition receptors (PRRs) on macrophages, thereby mediating endocytosis. PRRs include C-type lectin receptors, Toll-like receptors (TLRs), NOD-like receptors (NLRs), scavenger receptors, and Fc receptors.[73–75] Among them, C-type lectin receptors can recognize carbohydrate-rich molecules. The mannose receptor is one such C-type lectin receptor and can also recognize lipoarabinomannan on the cell wall of Mycobacterium tuberculosis (Mtb).[76] As a result, mannose has been widely used as a ligand to modify nanoparticle drug delivery systems in various studies. Chokshi et al[77] constructed rifampicin-loaded solid lipid nanoparticles with mannose surface modification. Flow cytometry analysis showed that mannose-modified solid lipid nanoparticles were significantly more efficiently internalized by macrophages compared to the unmodified nanoparticles. After incubation for 5 and 9 hours, the cellular uptake increased by 1.39 and 1.79 times, respectively, indicating that mannose modification enhances nanoparticle uptake by macrophages. The qualitative results from fluorescence microscopy were consistent with the quantitative flow cytometry data, showing that after 9 hours of incubation, macrophages internalized more mannose-modified nanoparticles than unmodified ones. Although the mannose molecule contains multiple hydroxyl functional groups, these hydroxyls provide abundant sites for coupling reactions with PLGA-PEG, allowing for ester linkage formation through esterification.[78] However, the stability of the ester bond formed is more susceptible to hydrolytic enzymes in the internal environment compared to amide bonds.[79] These enzymes can specifically catalyze the hydrolysis of ester bonds, leading to their cleavage, which results in the premature detachment of the ligand and consequently affects the targeting efficacy. In contrast, mannosamine, the amino derivative of mannose, has an amino group replacing one of the hydroxyl groups in mannose. Its chemical structure is more hydrophilic and reactive than mannose. Additionally, PLGA-PEG contains free carboxyl groups, which can chemically react with the amino group of mannosamine to form stable amide bonds.[80] Based on these findings, we selected mannosamine as the ligand for targeting macrophages in our nanoparticle formulation. In this study, to investigate the macrophage-targeting ability of MAN-PLGA-PEG NPs, we compared the uptake of MAN-PLGA-PEG NPs and PLGA-PEG NPs in RAW264.7 cells using flow cytometry. As shown in Figure 4C and D, the uptake of both NPs by RAW264.7 cells was time-dependent. However, the cellular uptake of MAN-PLGA-PEG NPs was significantly higher than that of PLGA-PEG NPs (Figures 4E and 5), indicating that mannose functionalization substantially enhanced the targeting efficiency of this PLGA-PEG nanosystem towards macrophages. At 24 hours, the macrophage uptake rate of MAN-PLGA-PEG was still four times higher than that of PLGA-PEG, which was significantly greater than the differences reported in the aforementioned literature. To further validate the role of D-mannosamine in the cellular uptake of NPs, we conducted free D-mannosamine competition experiments, demonstrating that the addition of free D-mannosamine inhibited the uptake of MAN-PLGA-PEG NPs in RAW264.7 cells (Figure 4F and G). These findings support the hypothesis that the selective uptake of MAN-PLGA-PEG NPs by macrophages is partially mediated by mannose receptor-dependent endocytosis.[81]

In vitro Anti-Tubercular Studies

The microplate-based Alamar Blue Assay (MABA) is a robust method for determining the inhibitory concentration of test formulations against M. tuberculosis. The minimum inhibitory concentration (MIC) was determined to identify the lowest concentrations of NPs and free RPT required to inhibit M. tuberculosis growth in vitro. As shown in Figure 6A, the MIC of free RPT was 0.2 μg/mL, while the MICs of RPT-PLGA-PEG NPs and RPT-MAN-PLGA-PEG NPs were both 0.047 μg/mL, which represents an approximately 4.25-fold reduction. This demonstrates that both nanoparticle formulations are significantly more effective than the free drug at inhibiting M. tuberculosis growth. The improved antimycobacterial activity of the NPs is likely due to their enhanced penetration through the mycobacterial cell wall, as

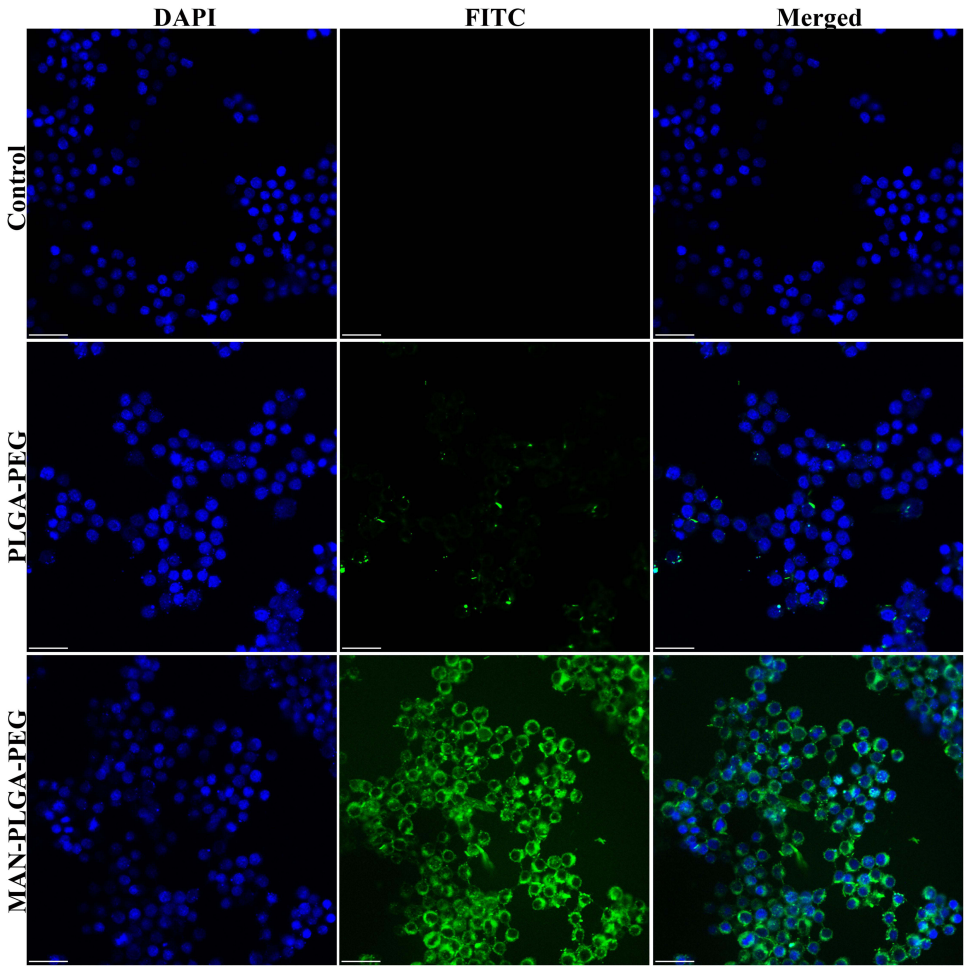

Figure 5 Fluorescence imaging of macrophages after 6 hours of co-incubation with PLGA-PEG and MAN-PLGA-PEG nanoparticles, captured using laser confocal microscopy. Blue is DAPI and green is nanoparticles carrying coumarin 6, scale bar: 25 μm, n=9.

NPs offer a higher surface area and more efficient delivery of RPT to its site of action, achieving equivalent efficacy at lower doses.

Intracellular Inhibition of Mycobacterium Tuberculosis Test

Currently, drug chemotherapy remains the primary treatment for tuberculosis(TB). The first-line anti-TB drugs commonly used in clinical practice primarily include streptomycin, isoniazid, and rifampicin, developed during the 1990s. However, the emergence of drug resistance, multidrug resistance, and co-infection with HIV has made the development of new anti-TB drugs an urgent global priority. In this study, rifapentine exhibited inhibitory effects against intracellular BCG and H37Rv, demonstrating superior antibacterial activity compared to rifampicin as reported by Pi et al.[63] Furthermore, the macrophage-targeting RPT-MAN-PLGA-PEG NPs significantly enhanced the intracellular antibacterial activity of rifapentine (Figure 6B and C).

Pharmacokinetics and Tissue Distribution Study

Figure 7A illustrates the serum concentration-time profile of the drug. In comparison to free RPT, which persisted in the system for only 2 days, the drug-loaded nanoparticles demonstrated an extended release profile. The key pharmacokinetic parameters are presented in Table 5. Both types of nanoparticles reduced the drug's plasma clearance rate compared to the free drug, as indicated by an increase in their half-lives by 1.76-fold and 2.03-fold for RPT-PLGA-PEG NPs and RPT-MAN-PLGA-PEG NPs, respectively. Importantly, the bactericidal efficacy of RPT is dependent on exposure time,

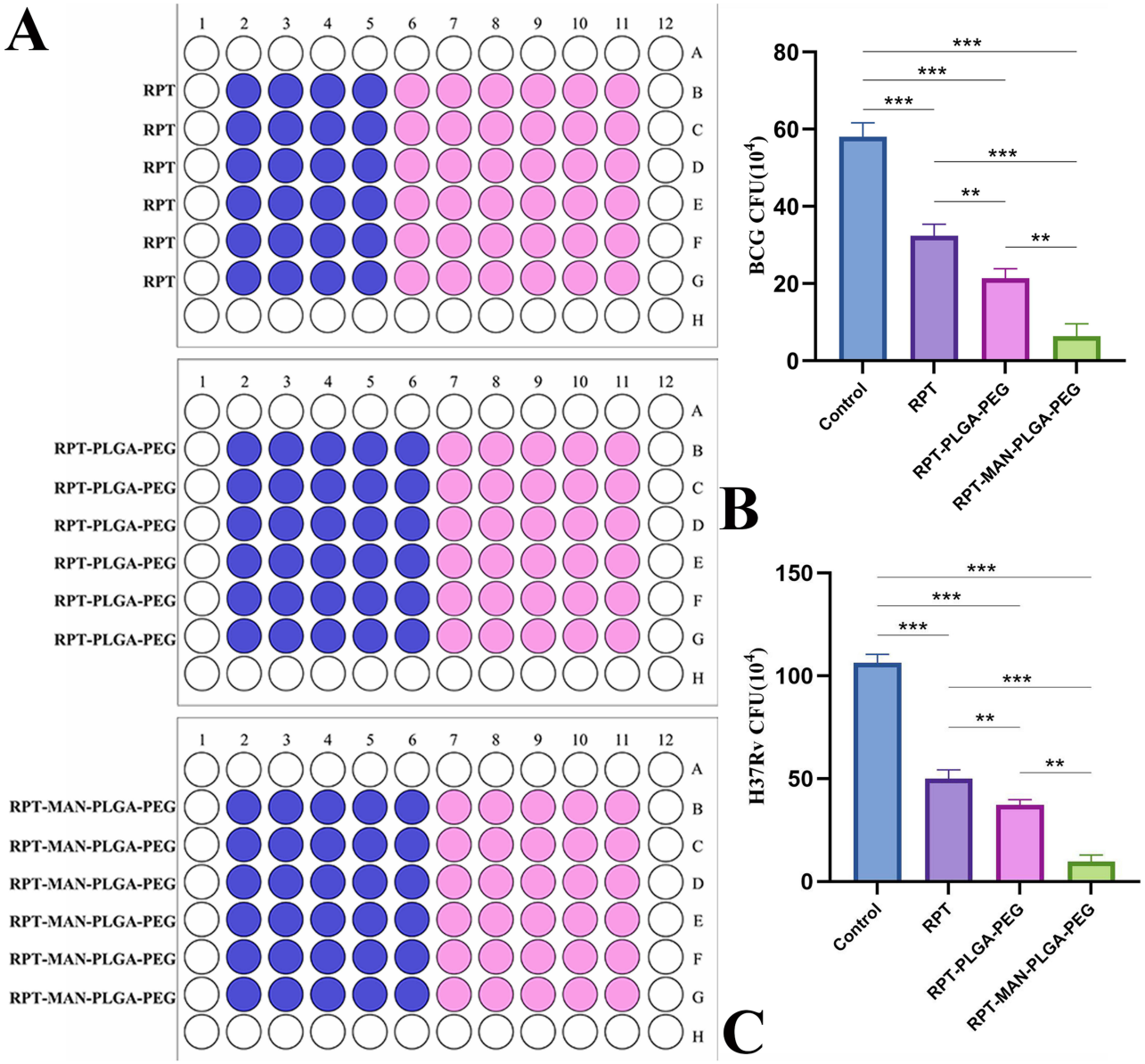

Figure 6 Bacteriostatic effect of nanomaterials (**A**) In vitro anti-tuberculosis study determining the minimum inhibitory concentration (MIC) of free rifapentine (RPT), RPT-PLGA-PEG, and RPT-MAN-PLGA-PEG nanoparticles (NPs). Pink indicates bacterial growth, while blue indicates the absence of bacterial growth, n=6. (**B**) Bactericidal effect of RPT-MAN-PLGA-PEG versus free rifapentine against BCG within RAW264.7. (**C**) Bactericidal effect of RPT-MAN-PLGA-PEG versus free rifapentine against H37Rv within RAW264.7, **P < 0.01, ***P < 0.001, n=6.

with the mean residence times (MRT) of RPT-PLGA-PEG NPs and RPT-MAN-PLGA-PEG NPs showing 1.95-fold (47.57 hours) and 2.22-fold (54.36 hours) increases, respectively, relative to a mere 24.38 hours for free RPT. A slow and sustained release profile of biodegradable nanoparticles is a critical feature for effective nanoparticle-mediated drug delivery. When administered in its free form, RPT rapidly attained high plasma concentrations within a few hours, followed by rapid degradation. Conversely, a single administration of the same RPT dose encapsulated in nanoparticles maintained plasma levels above the minimum inhibitory concentration (MIC) throughout all measured time points.

The distribution of RPT across different tissues is shown in Figure 7B. In the free RPT group, the concentration of the drug in the liver during the within one hour was significantly higher than that in the nanoparticle groups, suggesting a potential risk of hepatotoxicity. Over time, the RPT concentration gradually decreased as the drug was metabolized and cleared by the liver. The RPT-MAN-PLGA-PEG NPs demonstrated efficient localization in the lungs compared to free RPT and other nanoparticle formulations. The efficient localization of nanoparticles in the lungs can be attributed to the following: 1) Nanoparticles may

https://doi.org/10.2147/DDDT.S505682

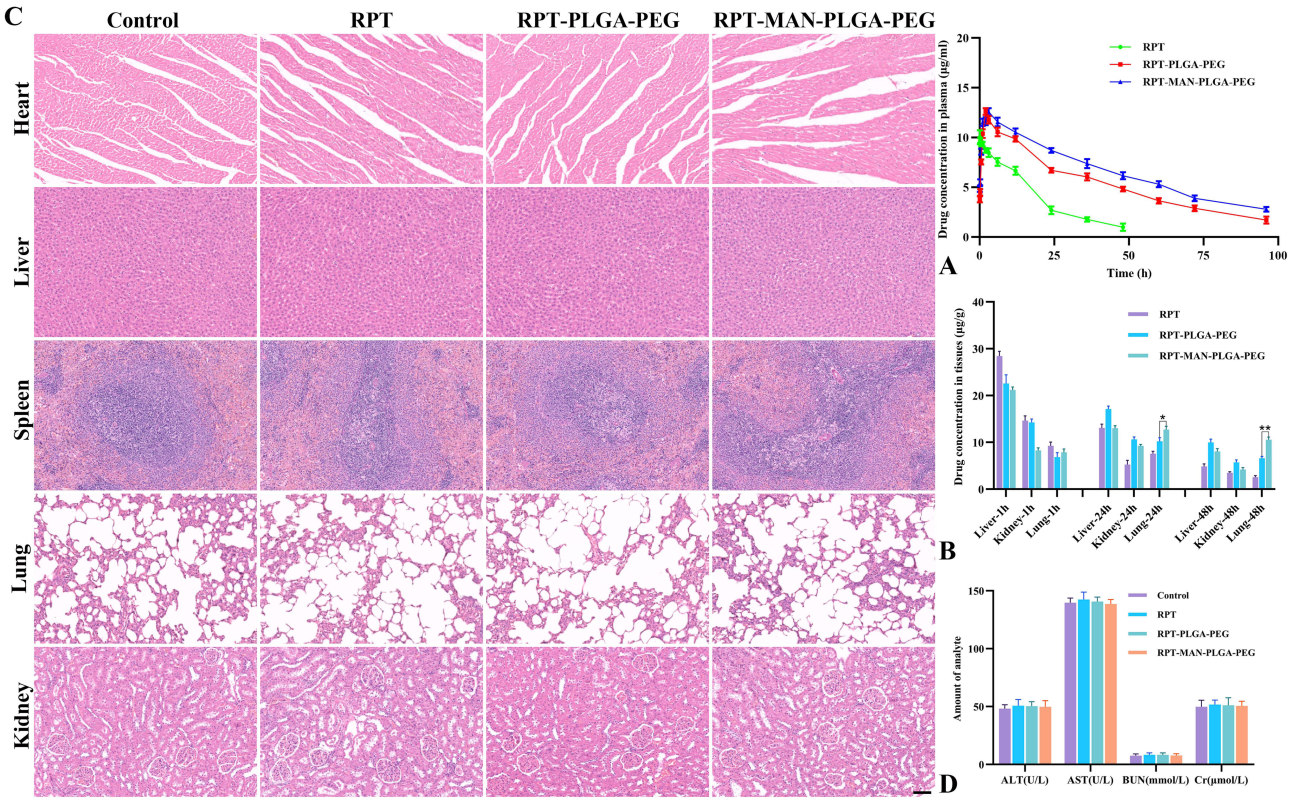

Figure 7 In vivo toxicity assessment and drug content analysis. (**A**) Plasma concentration-time profiles following administration of different drug formulations. (**B**) Drug distribution in the organs of SD rats. (**C**) Hematoxylin and eosin (H&E) staining of heart, liver, spleen, lung, and kidney tissues from SD rats, scale bar: 100 μm. (**D**) Serum biochemistry data for ALT, AST, Cr, and BUN levels, *P < 0.05, **P < 0.01, n=9.

be sequestered in the lungs after recirculation due to the filtration effects of lung capillaries. 2) Nanoparticles are likely cleared from the bloodstream through phagocytosis by cells of the pulmonary reticuloendothelial system. Mycobacterium tuberculosis primarily resides within lung macrophages, necessitating the delivery of RPT at bactericidal concentrations to the lungs for effective tuberculosis treatment.[82] Thus, RPT-MAN-PLGA-PEG NPs could serve as a promising strategy for delivering RPT to lung tissues.

Organ toxicity remains a significant challenge in the clinical use of antitubercular drugs. In this study, both histological and biochemical analyses were performed to assess the potential toxicity of the RPT-loaded NPs in comparison to the free drug. Major organs of mice were sectioned and subjected to histological analysis using H&E staining. The results showed no discernible abnormalities in the heart, spleen, liver, lungs, and kidneys across all four groups (free RPT, RPT-PLGA-PEG NPs, RPT-MAN-PLGA-PEG NPs, and controls) (Figure 7C). This suggests that the RPT-loaded NPs did not cause noticeable organ damage, supporting their potential safety for systemic administration. To evaluate the potential toxicity of the NPs further,

Table 5 Pharmacokinetic Parameters in Different Groups

	RPT	RPT-PLGA-PEG	RPT-MAN-PLGA-PEG
C_{max} (μg/mL)	9.39 ± 0.32	12.35 ± 0.57	13.31 ± 0.49
T_{max} (h)	0.083 ± 0.00	2.00 ± 0.00	3.00 ± 0.00
$t_{1/2}$ (h)	18.36 ± 6.41	32.37 ± 7.53	39.41 ± 5.76
$AUC_{0-\infty}$ (μg/mL h)	192.3 ± 12.13	411.48 ± 52.21	531.23 ± 47.76
MRT (h)	24.38 ± 4.76	47.57 ± 6.71	54.36 ± 5.43

Abbreviations: RPT, rifapentine; MAN, Mannosamine; PLGA, poly-d,l-lactide-co-glycolide; PEG, poly ethylene glycol; C_{max}, maximum concentration; T_{max}, time to reach peak plasma concentration; $t_{1/2}$, half life; $AUC_{0-\infty}$, area under the curve from 0 to ∞; MRT, mean residence time.

 https://doi.org/10.2147/DDDT.S505682

blood biochemical analysis was conducted to assess liver and kidney function. NPs are predominantly taken up and cleared by organs of the reticuloendothelial system (RES), such as the liver and kidneys.[83] Thus, alanine aminotransferase (ALT) and aspartate aminotransferase (AST) levels were measured to evaluate liver function, while blood urea nitrogen (BUN) and creatinine (Cr) levels were used as biomarkers for kidney function. All groups showed no significant differences when compared to the control group ($P > 0.05$) (Figure 7D). This suggests that the NPs did not induce any significant liver or kidney toxicity.

Conclusion

In this study, RPT-loaded MAN-PLGA-PEG NPs were prepared using an ultrasound emulsification method combined with solvent evaporation, with the goal of enhancing macrophage-targeting properties and improving anti-mycobacterial activity against Mycobacterium tuberculosis. The resulting nanoparticles exhibited favorable physicochemical properties, with no evidence of cytotoxicity or hemolytic toxicity, and demonstrated enhanced macrophage-targeting properties compared to PLGA-PEG NPs. In in vitro studies, RPT-loaded NPs demonstrated superior efficacy against Mtb compared to the free drug. Additionally, the NPs were well tolerated in rat models, showing a reduction in hepatotoxicity, suggesting that the NPs not only enhanced bactericidal efficacy but also offered improved safety profiles. Furthermore, the macrophage-targeting capabilities of the MAN-PLGA-PEG NPs allowed for effective drug delivery to macrophages, which are the primary host cells for Mtb, while enabling a reduction in dosing frequency as the NP-based formulations maintained therapeutic drug concentrations for extended periods. Consequently, the conventional daily administration of free RPT could potentially be replaced with intermittent dosing of these NP-based formulations, thereby improving patient adherence and reducing the risk of therapeutic failure and the development of drug resistance. In conclusion, RPT-loaded MAN-PLGA-PEG NPs represent a promising drug delivery system for tuberculosis treatment, combining enhanced bactericidal activity, macrophage-targeting efficiency, and reduced dosing frequency, making them an attractive alternative to conventional therapies.

Data Sharing Statement

The data sets generated and analyzed during the current study are not publicly available but can be obtained from the corresponding author on reasonable request.

Ethics Approval and Consent to Participate

The animal study was approved by the Ethics Committee of The Xinjiang Medical University (No. 20240711-18). The study was conducted in accordance with the local legislation and institutional requirements.

Author Contributions

All authors made a significant contribution to the work reported, whether that is in the conception, study design, execution, acquisition of data, analysis and interpretation, or in all these areas; took part in drafting, revising or critically reviewing the article; gave final approval of the version to be published; have agreed on the journal to which the article has been submitted; and agree to be accountable for all aspects of the work.

Funding

This work was supported by the National Natural Science Foundation of China (No.82172454).

Disclosure

The authors declare that they have no known competing financial interests or personal relationships that could have appeared to influence the work reported in this paper.

References

1. World Health Organization. Global tuberculosis report. (2024). Available from: https://www.who.int/publications/i/item/9789240101531. Accessed March 10, 2025.
2. Zhai W, Wu F, Zhang Y, Fu Y, Liu Z. The immune escape mechanisms of mycobacterium tuberculosis. *Int J mol Sci*. 2019;20(2):340. doi:10.3390/ijms20020340

3. Delogu G, Goletti D. The spectrum of tuberculosis infection: new perspectives in the era of biologics. *J Rheumatol Suppl*. 2014;91:11–16. doi:10.3899/jrheum.140097
4. Pai M, Behr MA, Dowdy D, et al. Tuberculosis. *Nat Rev Dis Primers*. 2016;2(1):16076. doi:10.1038/nrdp.2016.76
5. Yunus BR, Ss T, Doble M. Dual delivery of tuberculosis drugs via cyclodextrin conjugated curdlan nanoparticles to infected macrophages. *Carbohydr Polym*. 2019;218:53–62. doi:10.1016/j.carbpol.2019.04.056
6. Alfarisi O, Alghamdi WA, Al-Shaer MH, Dooley KE, Peloquin CA. Rifampin vs. rifapentine: what is the preferred rifamycin for tuberculosis? *Expert Rev Clin Pharmacol*. 2017;10(10):1027–1036. doi:10.1080/17512433.2017.1366311
7. Sheikhpour M, Delorme V, Kasaeian A, et al. An effective nano drug delivery and combination therapy for the treatment of Tuberculosis. *Sci Rep*. 2022;12(1):9591. doi:10.1038/s41598-022-13682-4
8. Liebenberg D, Gordhan BG, Kana BD. Drug resistant tuberculosis: implications for transmission, diagnosis, and disease management. *Front Cell Infect Microbiol*. 2022;12:943545. doi:10.3389/fcimb.2022.943545
9. Slj D, Patriota Y, de La Roca MF, Soares-Sobrinho JL. New perspectives in drug delivery systems for the treatment of tuberculosis. *Curr Med Chem*. 2022;29(11):1936–1958. doi:10.2174/0929867328666210629154908
10. Bourguignon T, Godinez-Leon JA, Gref R. Nanosized drug delivery systems to fight tuberculosis. *Pharmaceutics*. 2023;15(2):393. doi:10.3390/pharmaceutics15020393
11. Chae J, Choi Y, Tanaka M, Choi J. Inhalable nanoparticles delivery targeting alveolar macrophages for the treatment of pulmonary tuberculosis. *J Biosci Bioeng*. 2021;132(6):543–551. doi:10.1016/j.jbiosc.2021.08.009
12. Shen L, Liao K, Yang E, et al. Macrophage targeted iron oxide nanodecoys augment innate immunological and drug killings for more effective mycobacterium tuberculosis clearance. *J Nanobiotechnology*. 2023;21(1). doi:10.1186/s12951-023-02103-x.
13. Pi J, Chen D, Wang J, et al. Macrophage targeted graphene oxide nanosystem synergize antibiotic killing and host immune defense for Tuberculosis Therapy. *Pharmacol Res*. 2024;208:107379. doi:10.1016/j.phrs.2024.107379
14. Shao L, Shen S, Liu H. Recent advances in PLGA micro/nanoparticle delivery systems as novel therapeutic approach for drug-resistant tuberculosis. *Front Bioeng Biotechnol*. 2022;10:941077.
15. Wang Y, Xu Y, Song J, et al. Tumor cell-targeting and tumor microenvironment-responsive nanoplatforms for the multimodal imaging-guided photodynamic/photothermal/chemodynamic treatment of cervical cancer. *Int J Nanomed*. 2024;19:5837–5858. doi:10.2147/IJN.S466042
16. Tang J, Li J, Li G, et al. Spermidine-mediated poly(lactic-co-glycolic acid) nanoparticles containing fluorofenidone for the treatment of idiopathic pulmonary fibrosis. *Int J Nanomed*. 2017;12:6687–6704. doi:10.2147/IJN.S140569
17. Chen W, Li Y, Liu C, et al. In situ engineering of tumor-associated macrophages via a nanodrug-delivering-drug (beta-elemene@stanene) strategy for enhanced cancer chemo-immunotherapy. *Angew Chem Int Ed Engl*. 2023;62(41):e202308413. doi:10.1002/anie.202308413
18. Lin W, Fan S, Liao K, et al. Engineering zinc oxide hybrid selenium nanoparticles for synergetic anti-tuberculosis treatment by combining Mycobacterium tuberculosis killings and host cell immunological inhibition. *Front Cell Infect Microbiol*. 2023;12:1074533.
19. Wang H, Li B, Sun Y, et al. NIR-II AIE luminogen-based erythrocyte-like nanoparticles with granuloma-targeting and self-oxygenation characteristics for combined phototherapy of tuberculosis. *Adv Mater*. 2024;36(38):e2406143. doi:10.1002/adma.202406143
20. Choi S, Britigan BE, Moran DM, Narayanasamy P. Gallium nanoparticles facilitate phagosome maturation and inhibit growth of virulent Mycobacterium tuberculosis in macrophages. *PLoS One*. 2017;12(5):e0177987. doi:10.1371/journal.pone.0177987
21. Ma C, Wu M, Ye W, et al. Inhalable solid lipid nanoparticles for intracellular tuberculosis infection therapy: macrophage-targeting and pH-sensitive properties. *Drug Deliv Transl Res*. 2021;11(3):1218–1235. doi:10.1007/s13346-020-00849-7
22. Xu Y, Kim CS, Saylor DM, Koo D. Polymer degradation and drug delivery in PLGA-based drug-polymer applications: a review of experiments and theories. *J Biomed Mater Res B Appl Biomater*. 2017;105(6):1692–1716. doi:10.1002/jbm.b.33648
23. Ding D, Zhu Q. Recent advances of PLGA micro/nanoparticles for the delivery of biomacromolecular therapeutics. *Mater Sci Eng C Mater Biol Appl*. 2018;92:1041–1060. doi:10.1016/j.msec.2017.12.036
24. Bahlool AZ, Fattah S, O'Sullivan A, et al. Development of Inhalable ATRA-Loaded PLGA nanoparticles as host-directed immunotherapy against tuberculosis. *Pharmaceutics*. 2022;14(8):1745. doi:10.3390/pharmaceutics14081745
25. Mir M, Ahmed N, Rehman AU. Recent applications of PLGA based nanostructures in drug delivery. *Colloids Surf B Biointerfaces*. 2017;159:217–231. doi:10.1016/j.colsurfb.2017.07.038
26. Kim KT, Lee JY, Kim DD, Yoon IS, Cho HJ. Recent progress in the development of poly(lactic-co-glycolic acid)-based nanostructures for cancer imaging and therapy. *Pharmaceutics*. 2019;11(6):280. doi:10.3390/pharmaceutics11060280
27. Xu Q, Ensign LM, Boylan NJ, et al. Impact of surface Polyethylene Glycol (PEG) density on biodegradable nanoparticle transport in mucus ex vivo and distribution in vivo. *ACS Nano*. 2015;9(9):9217–9227. doi:10.1021/acsnano.5b03876
28. Cummings RD. The mannose receptor ligands and the macrophage glycome. *Curr Opin Struct Biol*. 2022;75:102394. doi:10.1016/j.sbi.2022.102394
29. Mukhtar M, Csaba N, Robla S, et al. Dry powder comprised of isoniazid-loaded nanoparticles of hyaluronic acid in conjugation with mannose-anchored chitosan for macrophage-targeted pulmonary administration in tuberculosis. *Pharmaceutics*. 2022;14(8):1543. doi:10.3390/pharmaceutics14081543
30. Prabhu P, Fernandes T, Chaubey P, et al. Mannose-conjugated chitosan nanoparticles for delivery of Rifampicin to Osteoarticular tuberculosis. *Drug Deliv Transl Res*. 2021;11(4):1509–1519. doi:10.1007/s13346-021-01003-7
31. Yang Z, Lou C, Wang X, et al. Preparation, characterization, and in-vitro cytotoxicity of nanoliposomes loaded with anti-tubercular drugs and TGF-beta1 siRNA for improving spinal tuberculosis therapy. *BMC Infect Dis*. 2022;22(1):824. doi:10.1186/s12879-022-07791-8
32. Grotz E, Tateosian N, Amiano N, et al. Nanotechnology in tuberculosis: state of the art and the challenges ahead. *Pharm Res*. 2018;35(11):213. doi:10.1007/s11095-018-2497-z
33. Jarvis B, Lamb HM. Rifapentine. *Drugs*. 1998;56(4):607–616. [discussion 617]. doi:10.2165/00003495-199856040-00008
34. Chan JG, Bai X, Traini D. An update on the use of rifapentine for tuberculosis therapy. *Expert Opin Drug Deliv*. 2014;11(3):421–431. doi:10.1517/17425247.2014.877886
35. Makadia HK, Siegel SJ. Poly Lactic-co-Glycolic Acid (PLGA) as biodegradable controlled drug delivery carrier. *Polymers (Basel)*. 2011;3(3):1377–1397. doi:10.3390/polym3031377
36. Wang J, Li J, Ren J. Surface modification of poly(lactic-co-glycolic acid) microspheres with enhanced hydrophilicity and dispersibility for arterial embolization. *Materials*. 2019;12(12):1959.

37. D'Souza AA, Shegokar R. Polyethylene glycol (PEG): a versatile polymer for pharmaceutical applications. *Expert Opin Drug Deliv*. 2016;13 (9):1257–1275. doi:10.1080/17425247.2016.1182485
38. Avgoustakis K. Pegylated poly(lactide) and poly(lactide-co-glycolide) nanoparticles: preparation, properties and possible applications in drug delivery. *Curr Drug Deliv*. 2004;1(4):321–333. doi:10.2174/1567201043334605
39. Zambito G, Deng S, Haeck J, et al. Fluorinated PLGA-PEG-mannose nanoparticles for tumor-associated macrophage detection by optical imaging and MRI. *Front Med Lausanne*. 2021;8. doi:10.3389/fmed.2021.712367
40. Praphakar RA, Munusamy MA, Alarfaj AA, Kumar SS, Rajan M. Zn^{2+} cross-linked sodium alginate-g-allylamine-mannose polymeric carrier of rifampicin for macrophage targeting tuberculosis nanotherapy. *New J Chem*. 2017;41(19):11324–11334. doi:10.1039/C7NJ01808H
41. Liang Q, Zhang P, Zhang L, et al. Development of tetracycline-modified nanoparticles for bone-targeted delivery of anti-tubercular drug. *Front Bioeng Biotechnol*. 2023;11:1207520.
42. Tariq M, Alam MA, Singh AT, Panda AK, Talegaonkar S. Surface decorated nanoparticles as surrogate carriers for improved transport and absorption of epirubicin across the gastrointestinal tract: pharmacokinetic and pharmacodynamic investigations. *Int J Pharm*. 2016;501(1–2):18–31. doi:10.1016/j.ijpharm.2016.01.054
43. D'Souza S, Du Plessis SM, Egieyeh S, et al. Physicochemical and biological evaluation of curdlan-poly(lactic-co-glycolic acid) nanoparticles as a host-directed therapy against mycobacterium tuberculosis. *J Pharm Sci*. 2022;111(2):469–478. doi:10.1016/j.xphs.2021.09.012
44. Nie Y, Li D, Peng Y, et al. Metal organic framework coated MnO(2) nanosheets delivering doxorubicin and self-activated DNAzyme for chemo-gene combinatorial treatment of cancer. *Int J Pharm*. 2020;585:119513. doi:10.1016/j.ijpharm.2020.119513
45. Liang Q, Xiang H, Li X, et al. Development of Rifapentine-Loaded PLGA-based nanoparticles: in vitro characterisation and in vivo study in mice. *Int J Nanomed*. 2020;15:7491–7507. doi:10.2147/IJN.S257758
46. Rani S, Gothwal A, Pandey PK, et al. HPMA-PLGA based nanoparticles for effective in vitro delivery of rifampicin. *Pharm Res*. 2019;36(1). doi:10.1007/s11095-018-2543-x.
47. Care NRCU, Animals AUOL. Guide for the Care and Use of Laboratory Animals. 2011.
48. Yang Y, Huang Z, Li J, et al. PLGA porous microspheres dry powders for codelivery of afatinib-loaded solid lipid nanoparticles and paclitaxel: novel therapy for EGFR tyrosine kinase inhibitors resistant nonsmall cell lung cancer. *Adv Healthc Mater*. 2019;8(23). doi:10.1002/adhm.201900965.
49. Tukulula M, Hayeshi R, Fonteh P, et al. Curdlan-conjugated PLGA nanoparticles possess macrophage stimulant activity and drug delivery capabilities. *Pharm Res*. 2015; 32:2713–2726.
50. Vieira AC, Magalhães J, Rocha S, et al. Targeted macrophages delivery of rifampicin-loaded lipid nanoparticles to improve tuberculosis treatment. *Nanomedicine (Lond)*. 2017;12(24):2721–2736. doi:10.2217/nnm-2017-0248
51. Carneiro SP, Carvalho KV, de Oliveira ASR, et al. Funct ionalized rifampicin-loaded nanostructured lipid carriers enhance macrophages uptake and antimycobacterial activity. *Colloids Surf B Biointerfaces*. 2019;175:306–313. doi:10.1016/j.colsurfb.2018.12.003
52. Rafiei P, Haddadi A. Docetaxel-loaded PLGA and PLGA-PEG nanoparticles for intravenous application: pharmacokinetics and biodistribution profile. *Int J Nanomed*. 2017;12:935–947. doi:10.2147/IJN.S121881
53. Rao J. Shedding light on tumors using nanoparticles. *ACS Nano*. 2008;2(10):1984–1986. doi:10.1021/nn800669n
54. Kircher MF, Mahmood U, King RS, Weissleder R, Josephson L. A multimodal nanoparticle for preoperative magnetic resonance imaging and intraoperative optical brain tumor delineation. *Cancer Res*. 2003;63(23):8122–8125.
55. Owens DR, Peppas NA. Opsonization, biodistribution, and pharmacokinetics of polymeric nanoparticles. *Int J Pharm*. 2006;307(1):93–102. doi:10.1016/j.ijpharm.2005.10.010
56. Liu Y, Wu X, Mi Y, et al. PLGA nanoparticles for the oral delivery of nuciferine: preparation, physicochemical characterization and in vitro/in vivo studies. *Drug Deliv*. 2017;24(1):443–451. doi:10.1080/10717544.2016.1261381
57. Yoo JW, Chambers E, Mitragotri S. Factors that control the circulation time of nanoparticles in blood: challenges, solutions and future prospects. *Curr Pharm Des*. 2010;16(21):2298–2307. doi:10.2174/138161210791920496
58. Wang J, Sui M, Fan W. Nanoparticles for tumor targeted therapies and their pharmacokinetics. *Curr Drug Metab*. 2010;11(2):129–141. doi:10.2174/138920010791110827
59. Haggag Y, Abdel-Wahab Y, Ojo O, et al. Preparation and in vivo evaluation of insulin-loaded biodegradable nanoparticles prepared from diblock copolymers of PLGA and PEG. *Int J Pharm*. 2016;499(1–2):236–246. doi:10.1016/j.ijpharm.2015.12.063
60. Mahanta AK, Chaulagain B, Trivedi R, Singh J. Mannose-functionalized chitosan-coated PLGA nanoparticles for brain-targeted codelivery of CBD and BDNF for the treatment of Alzheimer's disease. *ACS Chem Neurosci*. 2024;15(21):4021–4032. doi:10.1021/acschemneuro.4c00392
61. Singodia D, Verma A, Verma RK, Mishra PR. Investigations into an alternate approach to target mannose receptors on macrophages using 4-sulfated N-acetyl galactosamine more efficiently in comparison with mannose-decorated liposomes: an application in drug delivery. *Nanomed Nanotechnol Biol Med*. 2012;8(4):468–477. doi:10.1016/j.nano.2011.07.002
62. Magalhaes J, Cl L, Va C, et al. Optimization of rifapentine-loaded lipid nanoparticles using a quality-by-design strategy. *Pharmaceutics*. 2020;12 (1). doi:10.3390/pharmaceutics12010075.
63. Pi J, Shen L, Shen H, et al. Mannosylated graphene oxide as macrophage-targeted delivery system for enhanced intracellular M.tuberculosis killing efficiency. *Mater Sci Eng C*. 2019;103:109777. doi:10.1016/j.msec.2019.109777
64. Hetta HF, Ahmed EA, Hemdan AG, et al. Modulation of rifampicin-induced hepatotoxicity using poly(lactic-co-glycolic acid) nanoparticles: a study on rat and cell culture models. *Nanomedicine (Lond)*. 2020;15(14):1375–1390. doi:10.2217/nnm-2020-0001
65. Jahagirdar PS, Gupta PK, Kulkarni SP, Devarajan PV. Intramacrophage delivery of dual drug loaded nanoparticles for effective clearance of mycobacterium tuberculosis. *J Pharm Sci*. 2020;109(7):2262–2270. doi:10.1016/j.xphs.2020.03.018
66. Wei Y, Liang J, Zheng X, et al. Lung-targeting drug delivery system of baicalin-loaded nanoliposomes: development, biodistribution in rabbits, and pharmacodynamics in nude mice bearing orthotopic human lung cancer. *Int J Nanomed*. 2017;12:251–261. doi:10.2147/IJN.S119895
67. Tao Y, Jiao G, Zhao X, et al. Amino acid-crosslinked 4arm-PLGA Janus patch with anti-adhesive and anti-bacterial properties for hernia repair. *Colloids Surf. B*. 2024;243:114126. doi:10.1016/j.colsurfb.2024.114126
68. Singh SK, Singh S, Lillard JJ, Singh R. Drug delivery approaches for breast cancer. *Int J Nanomed*. 2017;12:6205–6218. doi:10.2147/IJN.S140325
69. Li M, Tang Z, Lv S, et al. Cisplatin crosslinked pH-sensitive nanoparticles for efficient delivery of doxorubicin. *Biomaterials*. 2014;35 (12):3851–3864. doi:10.1016/j.biomaterials.2014.01.018

70. Pourjavadi A, Tehrani ZM. Mesoporous silica nanoparticles with bilayer coating of poly(acrylic acid-co-itaconic acid) and human serum albumin (HSA): a pH-sensitive carrier for gemcitabine delivery. *Mater Sci Eng C Mater Biol Appl*. 2016;61:782–790. doi:10.1016/j.msec.2015.12.096
71. Silva AC, Kumar A, Wild W, et al. Long-term stability, biocompatibility and oral delivery potential of risperidone-loaded solid lipid nanoparticles. *Int J Pharm*. 2012;436(1–2):798–805. doi:10.1016/j.ijpharm.2012.07.058
72. Costa P, Sousa LJ. Modeling and comparison of dissolution profiles. *Eur J Pharm Sci*. 2001;13(2):123–133. doi:10.1016/S0928-0987(01)00095-1
73. Paurević M, Šrajer Gajdošik M, Ribić R. Mannose ligands for mannose receptor targeting. *Int J mol Sci*. 2024;25(3):1370. doi:10.3390/ijms25031370
74. Krishnan V, Nath S, Nair P, Das B. Mycobacterium tuberculosis and its clever approaches to escape the deadly macrophage. *World J Microbiol Biotechnol*. 2023;39(11). doi:10.1007/s11274-023-03735-9
75. Lin W, Shen C, Li M, et al. Programmable macrophage vesicle based bionic self-adjuvanting vaccine for immunization against monkeypox virus. *Adv Sci*. 2024;12(1):e2408608. doi:10.1002/advs.202408608
76. Hmama Z, Pena-Diaz S, Joseph S, Av-Gay Y. Immunoevasion and immunosuppression of the macrophage by Mycobacterium tuberculosis. *Immunol Rev*. 2015;264(1):220–232. doi:10.1111/imr.12268
77. Chokshi NV, Rawal S, Solanki D, et al. Fabrication and characterization of surface engineered rifampicin loaded lipid nanoparticulate systems for the potential treatment of tuberculosis: an in vitro and in vivo evaluation. *J Pharm Sci*. 2021;110(5):2221–2232. doi:10.1016/j.xphs.2021.02.018
78. Fan Z, Wang Y, Xiang S, et al. Dual-self-recognizing, stimulus-responsive and carrier-free methotrexate-mannose conjugate nanoparticles with highly synergistic chemotherapeutic effects. *J Mater Chem B*. 2020;8(9):1922–1934. doi:10.1039/D0TB00049C
79. Hofmann J, Spatz P, Walther R, et al. Synthesis and biological evaluation of flavonoid-cinnamic acid amide hybrids with distinct activity against neurodegeneration in vitro and in vivo. *Chemistry*. 2022;28(39):e202200786. doi:10.1002/chem.202200786
80. Li X, Xiu X, Su R, et al. Immune cell receptor-specific nanoparticles as a potent adjuvant for nasal split influenza vaccine delivery. *Nanotechnology*. 2024;35(12): 125101.
81. Pi J, Shen L, Yang E, et al. Macrophage-targeted isoniazid–selenium nanoparticles promote antimicrobial immunity and synergize bactericidal destruction of tuberculosis bacilli. *Angew Chem*. 2020;132(8):3252–3260. doi:10.1002/ange.201912122
82. Liu Z, Li X, Xiu B, et al. A novel and simple preparative method for uniform-sized PLGA microspheres: preliminary application in antitubercular drug delivery. *Colloids Surf B Biointerfaces*. 2016;145:679–687. doi:10.1016/j.colsurfb.2016.05.085
83. Ganipineni LP, Ucakar B, Joudiou N, et al. Magnetic targeting of paclitaxel-loaded poly(lactic-co-glycolic acid)-based nanoparticles for the treatment of glioblastoma. *Int J Nanomed*. 2018;13:4509–4521. doi:10.2147/IJN.S165184